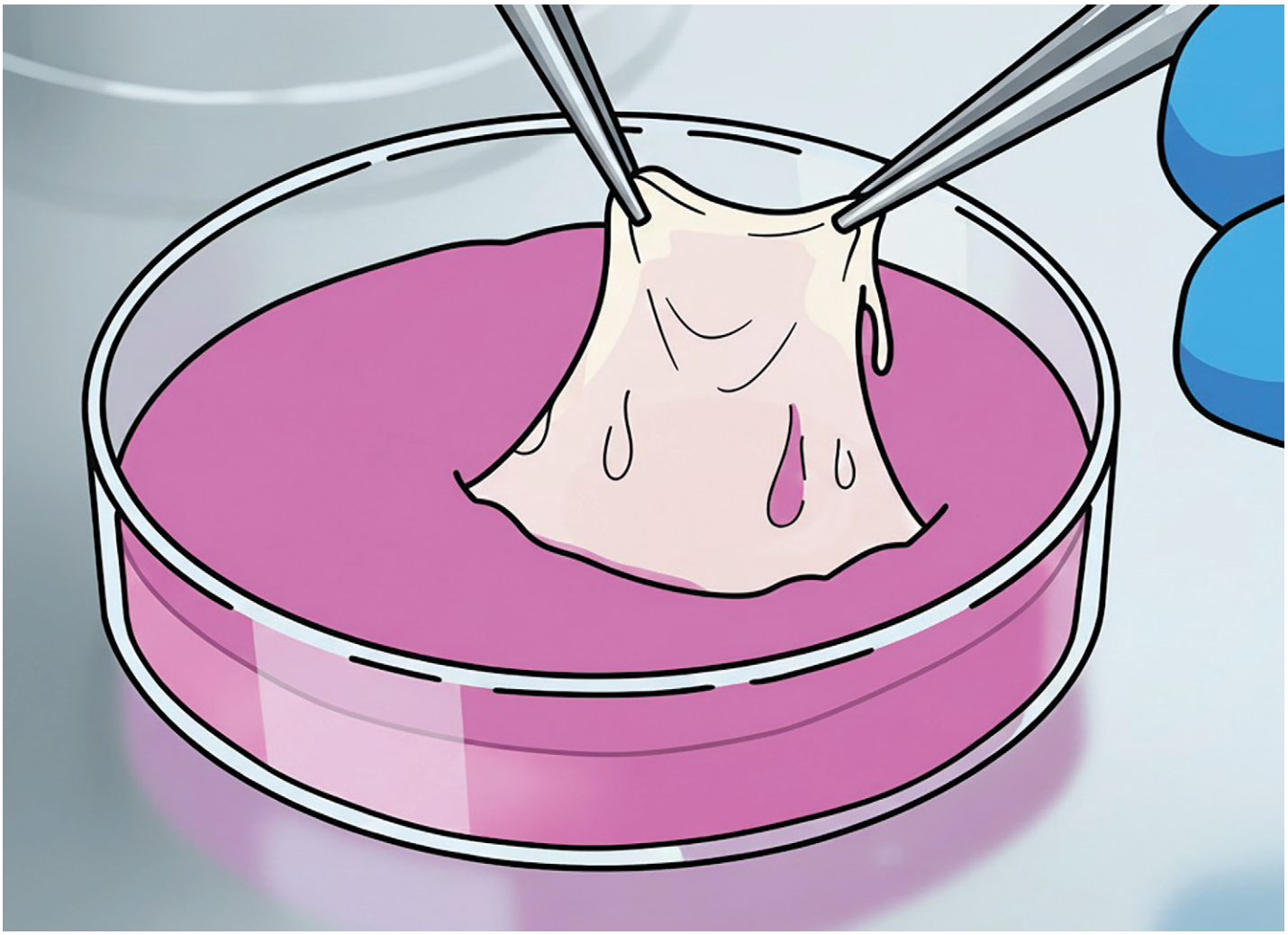

Showcasing research from Professor P. Ravi Selvaganapathy's laboratory, School of Biomedical Engineering, McMaster University, Ontario, CANADA.

Rapid Scaffold-Free Cell Sheet Formation and Their Patterning as Building Blocks of Complex 3D Tissue Constructs

In this paper, we describe a seemingly simple yet surprising method to form large area cell sheets within 4-6 hours by leveraging cells' natural adhesion to each other. We also show that building blocks made from these cell sheets can be used to assemble complex shapes and structures. Finally, we apply this technology to make skin from burn derived stem cells and demonstrate their wound healing properties in an animal model.

Image reproduced by permission of P. Ravi Selvaganapathy from *Lab Chip*, 2026, **26**, 286.

As featured in:

See P. Ravi Selvaganapathy *et al.*, *Lab Chip*, 2026, **26**, 286.

ROYAL SOCIETY OF CHEMISTRY

rsc.li/loc

Registered charity number: 207890

Lab on a Chip

ROYAL SOCIETY OF CHEMISTRY

PAPER

View Article Online
View Journal | View Issue

Cite this: *Lab Chip*, 2026, **26**, 286

Rapid scaffold-free cell sheet formation and their patterning as building blocks of complex 3D tissue constructs

Maedeh Khodamoradi, [a] Seyedaydin Jalali, [ae] Maria Fernanda Hutter,[abc] Yufei Chen,[abc] Faraz Chogan,[d] Alisa Douglas,[abc] Graham Rix,[abc] Bhavishya Challagundla,[abc] Margarita Elloso,[abc] Marc G. Jeschke[abcd] and P. Ravi Selvaganapathy *[ae]

Three-dimensional (3D) cell cultures offer superior potential in replicating native tissue microenvironments by better supporting cell–cell and cell–extracellular matrix (ECM) interactions that are critical for guiding cellular behavior and functionality in engineered tissues. Among 3D approaches, scaffold-free techniques have gained attention for their ability to produce high-cellular density, and well-organized tissue-like constructs. In particular, cell sheets are uniquely suited for regenerative applications due to their contiguous architecture, large-area coverage, and integration potential with host tissues. However, current biofabrication methods for cell sheet production often require altering culture conditions (*e.g.*, temperature, pH) or applying external stimuli (*e.g.*, magnetic or electrical fields), which can damage cells, compromise sheet integrity, or demand costly, non-adaptable equipment. Here, we present a rapid, self-assembly-based technique using unmodified polydimethylsiloxane (PDMS) molds as culture vessels. When seeded at a critical cell density, adherent cells spontaneously self-assemble into planar 3D cell sheets within 6 hours, without substrate modification or specialized equipment. Our qRT-PCR analysis revealed significant upregulation of E-cadherin in cell sheets, confirming that cell–cell adhesion, rather than cell-substrate anchorage, drives sheet formation. We showed that our technique is versatile, supporting the creation of large-area and patterned sheets, stacked multi-layer constructs, and co-culture configurations. Notably, fibroblast cell sheets, demonstrated progressive ECM production, with histological analysis confirming collagen deposition over time. Overall, our approach preserves cell viability and function while offering a simple, rapid, and cost-effective alternative to conventional methods for fabricating cell sheets. This platform holds broad potential for applications in tissue engineering, regenerative medicine, disease modeling, and cultivated meat production.

Received 8th July 2025,
Accepted 2nd December 2025

DOI: 10.1039/d5lc00678c

rsc.li/loc

Introduction

In regenerative medicine, effective cell delivery, as the bioactive component of the tissue, is crucial for tissue regeneration and is typically achieved through cell suspension injection, scaffold-based, or scaffold-free approaches.[1] While direct cell suspension injection is widely used, it often shows low therapeutic efficacy due to poor cell survival and retention (often fewer than 5%) at the injury site.[2,3] Scaffold-based tissue engineering aims to improve delivery using biocompatible, biodegradable materials to create 3D grafts;[4] however, challenges such as low cellular density (1–10 million cells per mL *vs.* 1–3 billion cells per mL in native tissues) and potential immunotoxicity from exogenous scaffolds limit their clinical translation.[1,5,6]

To overcome these issues, scaffold-free strategies have been developed, allowing cells to form high cell density tissue analogs by producing their own ECM, reducing immune risks, and supporting natural interactions.[1,7] Techniques such as cellular spheroids,[8] magnetically induced aggregation,[9] and cell sheet engineering[10] have emerged to achieve this. Spheroids, dense microscale aggregates, offer enhanced cell survival, signaling, and angiogenesis post-transplantation.[11] Yet, their clinical use is limited by difficulties in mass production, size control, and delivery challenges.[11] While non-adhesive plates enable large-scale generation, they lack control over spheroid

[a] *School of Biomedical Engineering, McMaster University, Hamilton, ON, Canada. E-mail: selvaga@mcmaster.ca*
[b] *Department of Surgery, McMaster University, Hamilton, ON, Canada*
[c] *Hamilton Health Sciences Centre, Thrombosis and Atherosclerosis Research Institute, Hamilton, ON, Canada*
[d] *Institute of Medical Science, University of Toronto, Toronto, ON, Canada*
[e] *Department of Mechanical Engineering, McMaster University, Hamilton, ON, Canada*

uniformity. Other methods, such as hanging drops, spin flasks, and microwells, also suffer from scalability, reduced viability, and cost, respectively.[11] Furthermore, similar to single cell suspension, spheroid retention at the site of injury remains problematic. To address this, secondary compaction strategies have been explored to post-assemble spheroids into larger constructs using porous scaffolds or bioinks.[12] Magnetically induced aggregation techniques further offer control over spheroid size, shape, and patterning by introducing magnetic nanoparticles before or after aggregation.[13] While promising for *in vitro* modeling, these require multi-step procedures, specialized bioreactors, and external materials that may affect native cell behavior.

Cell sheet engineering was developed to overcome these limitations. Cell sheets are contiguous, planar, cell-only constructs composed of one to several layers of densely packed cells, forming ~10–100 μm-thick tissues.[14–16] Their thickness can exceed this range by increasing cell number or stacking multiple sheets; however, due to transport limitations in thicker constructs,[17] properly engineered sheets generally remain within this range. Cell densities in engineered cell sheets are commonly on the order of 10^8–10^9 cells per mL representing a high cellular density that is comparable to those of native tissue subunits,[6,14,18–20] and higher than in many conventional tissue-engineered constructs produced by techniques such as hydrogel-based extrusion bioprinting or cell-laden porous scaffolds.[5,21–23]

In most cell sheet fabrication approaches, cells are cultured to confluence (typically 10^5–10^6 cells per cm^2), during which they establish intercellular junctions and produce their own ECM.[24] The cohesive cell sheet is then lifted off as a single, intact 3D structure, while maintaining the natural interactions between cells and the ECM.[24] These patch-like constructs provide a homogeneous distribution of cells and ECM, enabling consistent delivery of regenerative cues and improving suitability for transplantation.[24] Compared with single-cell suspension injection, where cells often form unorganized clusters or remain isolated, cell sheets show superior structural integrity and bioactivity, promoting more uniform integration with host tissue.[10,25]

The most common fabrication approach uses temperature-responsive surfaces (*e.g.*, PIPAAm-coated plates), where reduced temperature alters surface hydrophilicity to induce cell sheet detachment.[26] Although this technique maintains ECM and viability, it is highly sensitive to temperature control. Failure to meet the optimal condition may disturb the delamination or compromise sheet integrity. Moreover, long delamination process that requires 40–80 minutes at 20 °C, can negatively impact cell function. Other methods induce delamination by altering the culture medium pH to acidic levels (pH 4–6).[14,27] While effective in some cases, this chemical stress can impair cell viability and protein expression, hinder large-area detachment, and limit the range of compatible cell types.

To avoid altering culture conditions, other systems apply external stimuli such as electrical or light signals to trigger detachment. These require surface modification prior to cell seeding. For instance, in electro-responsive systems, cells grow on a gold-treated substrate, and an applied negative electric field releases the cell sheet within a short period.[28] Despite its rapid processing time, this method requires extensive surface modification, specialized equipment, and the design of cell-specific ligands, all of which can substantially increase costs and hinder its broader adoption. Local pH changes from polyelectrolyte dissolution may also damage sensitive cells.[24] Photo-responsive systems use TiO_2 nanodot-coated quartz substrates, where UV light alters surface wettability to enable cell sheet detachment.[29] However, the underlying mechanism remains unclear, and its compatibility across various cell types is yet to be validated.[24] Overall, these systems share two major drawbacks: (1) a multi-step fabrication process, first establishing cell–cell and ECM interactions in 2D, followed by a detachment step that prolongs the culture period to achieve the desired integrity and confluency for an intact delaminated cell sheet; and (2) reliance on conventional 2D culture, which does not replicate the native cellular environment and may compromise ECM secretion and cellular function.[30]

In this study, we present a simple, single-step method for fabricating 3D cell sheets, enabling rapid formation of robust, planar constructs without the need for substrate modification, altering the culture condition, or applying external stimuli. By seeding cells at a critical density, near monolayer coverage, onto pristine PDMS molds, the low surface energy of PDMS minimizes cell–substrate adhesion and promotes cell–cell interactions, as indicated by elevated E-cadherin expression, which highlights the key role of intercellular junctions in sheet formation. Furthermore, viability assays and Picrosirius Red (PSR) staining demonstrated that our method maintains high cell viability and supports ECM production, respectively. We further demonstrated the versatility of this technique by showing its ability to produce cell sheets that conform to the geometry of the mold, enabling the fabrication of customized patches or modular units for complex tissue assembly. This method was successfully applied across a broad range of cell types, including established cell lines, primary cells, and stem cells derived from mouse, bovine, and human sources, underscoring its adaptability. Additionally, we demonstrated its capability for spatial patterning and co-culture, facilitating the fabrication of heterogeneous cell sheets. Ultimately, this accessible and cost-effective technique enables rapid generation of functional cell sheets in standard lab settings, with potential applications in regenerative medicine, *in vitro* modeling, and clinical grafting.

Experimental

PDMS mold fabrication

The cell sheet fabrication process begins with the preparation of pristine polydimethylsiloxane (PDMS) molds in shapes and

sizes representing the final geometry of the cultivated cell sheets. Negative designs of the desired features were created using SolidWorks® software, and acrylonitrile butadiene styrene (ABS) master molds were 3D printed. A 10 : 1 mixture of PDMS base (Dow Corning Sylgard 184) and its curing agent was prepared and degassed under vacuum for 1 hour. The degassed mixture was then cast onto the 3D-printed master molds, cured at 80 °C for 2 hours, and peeled off to obtain the final PDMS molds. For sterilization, the molds were heated to 120 °C for 10 minutes, sprayed with 70% ethanol, and left to dry inside a biosafety cabinet (BSC) before use in cell culture. Molds of various shapes including circle, square, rectangle, cross, star, and dumbbell were fabricated for this study.

Cell culture

Various cell lines were cultured in standard polystyrene tissue culture plates prior to detachment and use in scaffold-free cell sheet fabrication. Green fluorescent protein (GFP)-expressing NIH-3T3 fibroblasts (Cell Biolabs, Cat#: AKR-214) and NIH/3T3 cells (ATCC, Cat#: CRL-1658) were used as the main cell sources and cultured in high-glucose Dulbecco's Modified Eagle Medium (DMEM, Gibco™ Cat#: 11965092) supplemented with 10% (v/v) fetal bovine serum (FBS, Gibco™ Cat#: 12483020) and 1% (v/v) penicillin–streptomycin (10 000 U mL^{-1}, Gibco™ Cat#: 15140122).

Other adherent cell types were cultured in their respective culture media. C2C12 mouse myoblasts were maintained in high-glucose DMEM (Gibco™ Cat#: 11965092) with 10% (v/v) heat-inactivated FBS (HI-FBS, Gibco™ Cat#: 12484028) and 1% penicillin–streptomycin. 3T3-L1 mouse preadipocytes were cultured in low-glucose DMEM + GlutaMAX (Gibco™ Cat#: 10567014) supplemented with 10% HI-FBS and 1% penicillin–streptomycin. Human skeletal muscle cells (HSKMCs) were expanded in ready-to-use growth medium (PromoCell Cat#: C-23060) and differentiated using the manufacturer's differentiation medium (PromoCell Cat#: C-23061). SaOs-2 human osteosarcoma cells were cultured in McCoy's 5A Modified Medium (Gibco™ Cat#: 16600082) containing 15% FBS and 1% penicillin–streptomycin. BeWo human placental choriocarcinoma cells were maintained in Ham's F-12 K (Kaighn's) medium (Gibco™ Cat#: 21127022) supplemented with 10% FBS and 1% penicillin–streptomycin.

Red fluorescent protein (RFP)-tagged human umbilical vein endothelial cells (HUVECs) were cultured in Endothelial Cell Growth Medium 2 (EGM2, PromoCell Cat#: C-22011). Primary bovine satellite cells (Opo-Moo-M17, Opo Bio, New Zealand) were cultured in Ham's F-10 Nutrient Mix (Gibco™ Cat#: 11550043) containing 20% FBS, 0.625 μg mL^{-1} amphotericin B (Gibco™ Cat#: 15290026), 1% penicillin–streptomycin, and 5 ng mL^{-1} recombinant human bFGF (Gibco™ Cat#: PHG0367).

Human burn-derived mesenchymal stem cells (BD-MSCs), umbilical cord-derived MSCs (UC-MSCs), and normal human skin fibroblasts (NF) were kindly provided by Dr. Marc G. Jeschke's research group (David Braley Research Institute, McMaster University). BD-MSCs and NF were cultured in CTS™ KnockOut™ DMEM/F12 (Gibco™ Cat#: A1370801) supplemented with 10% FBS and 1% antibiotic–antimycotic (Gibco™ Cat#: 15240112). UC-MSCs were cultured in the same basal medium supplemented with 10% FBS, 1% antibiotic–antimycotic, and 1% MEM Non-Essential Amino Acids (NEAA, Gibco™ Cat#: 11140076).

Cell sheet formation

Scaffold-free cell sheet formation began with the detachment of GFP-expressing NIH/3T3 fibroblasts from standard tissue culture plates using trypsin when cultures reached 80–90% confluency. To determine the optimal cell number for generating a continuous and thin cell sheet, cells were counted, and aliquots ranging from 0.3×10^6 to 2×10^6 cells were prepared. These were centrifuged, resuspended in 300 μL of growth medium, and added into circular PDMS molds (1 cm diameter), followed by incubation at 37 °C with 5% CO_2. The same protocol was applied to fabricate cell sheets from six additional cell types described in the section titled 'Cell culture'.

To evaluate sheet formation and optimize seeding density, brightfield imaging was performed after 1 day of incubation using a stereo microscope (Infinity Optical Systems). Additional images were taken at 6 hours, and on days 1, 2, and 4 to monitor contraction behaviour of the optimized cell sheets during the culture period. The contraction rate of the cell sheets was analyzed using ImageJ software.

Scalability of cell sheet manufacturing and assembly to form complex structures

To evaluate the scalability of the cell sheet biofabrication technique, three strategies were employed: fabrication of larger sheets, stacking of individual sheets, and modular "Lego-like" assembly of multiple sheets into complex structures. To fabricate larger sheets, circular PDMS molds of various diameters (2, 3, and 8 cm), were fabricated following the protocol described in the section titled 'PDMS mold fabrication'. For each mold, the approximate seeding density required to form a continuous sheet was calculated using the equation below, based on the optimized seeding density (OSD) determined for the 1 cm circular mold:

$$\text{Seeding density} = (\text{Surface area of new mold in cm}^2/0.785\ \text{cm}^2) \times \text{OSD} \quad (1)$$

As the second strategy, thicker, tissue-like constructs were created by vertically stacking two (double-layer) or three (triple-layer) individual cell sheets. Stacking was performed in standard 24-well plates containing 2 mL of growth medium. Cell sheets (day 1) were manually transferred using tweezers and placed directly on top of one another. The medium was then carefully aspirated to allow the sheets to settle and make initial close contact by gravity for 15 minutes, after which 2 mL of fresh medium was gently added. Brightfield images were captured immediately after

stacking (D1), and again on days 2 and 4 using the stereo microscope. ImageJ software was used to measure sheet diameter and analyze shrinkage behavior as a function of sheet number.

To fabricate more complex macrostructures, dumbbell-shaped and square sheets were fabricated and used as modular units. These were assembled into larger structures by overlapping their ends inside 24-well plates containing sufficient culture medium. Sheets were positioned using tweezers, and most of the medium was gently removed to promote contact at overlapping regions without disturbing the pattern. After a 15-minute incubation, 2 mL of fresh medium was added to each well. Structural integrity and mechanical stability of the assembled constructs were assessed after 1 day by manual handling.

Patterning and making multicellular cell sheets

To investigate the feasibility of creating spatially organized and multicellular cell sheets, several patterning strategies were developed using NIH-3T3 fibroblasts. Cells were cultured to approximately 90% confluency and stained with DiO or DiL fluorescent cell trackers (Thermo Fisher Scientific) following the manufacturers instruction to enable visualization of their distribution within the final constructs using either inverted fluorescence microscope (Ti2 Nikon) or Chemidock imager. After staining, cells were trypsinized, resuspended in culture medium, and used in the following procedures.

To fabricate bilayer co-culture sheets, 1.5×10^6 DiL-stained NIH-3T3 cells were seeded into a 1 cm diameter circular PDMS mold and incubated for 30 minutes at 37 °C and 5% CO_2 to allow initial cell settling. After gentle removal of excess medium, 1.5×10^6 DiO-stained NIH-3T3 cells were added on top of the first layer, followed by incubation for 24 hours to allow full sheet formation and layer integration (Fig. S1a).

For mixed co-culture sheets, equal numbers of DiO- and DiL-labeled NIH-3T3 cells (0.75×10^6 each) were resuspended in the culture medium and simultaneously seeded into the PDMS mold. Samples were incubated at 37 °C with 5% CO_2 for 24 hours to allow self-assembly into a homogeneous sheet.

To generate patterned sheets using geometric confinement, dumbbell-shaped PDMS molds were used. DiO- and DiL-stained NIH-3T3 cell suspensions were subsequently added into each region of the mold with 15 minutes intervals while the excessed medium in the first region gently removed before adding the cell suspension to the second region (Fig. S1b). The mold's geometry and the hydrophobic PDMS surface restricted mixing between compartments. Samples were incubated for 24 hours under standard culture conditions.

For partitioned patterning, a 3D-printed polylactic acid (PLA) insert with a 600 μm partition wall thickness was placed inside a 1 cm diameter circular PDMS mold to create two isolated compartments. DiO- and DiL-stained NIH-3T3 cells (0.75×10^6 each) were seeded into the respective regions simultaneously (Fig. S1c). After 15 minutes of cell settling, the insert was gently removed, and the partitioned cell populations were incubated for another 24 hours to allow integration of both populations into a continuous patterned sheet.

Freehand and marbled patterning strategies were also performed. For freehand pipetting, rectangular PDMS molds (2 × 4 cm) were fabricated and used as the patterning substrate. A total of 4×10^6 DiL-labeled NIH-3T3 cells were resuspended in 400 μL of culture medium. Using a fine-tip pipette, 200 μL of the cell suspension was drawn across the PDMS surface to form a straight line (Fig. S1d). The remaining suspension was then used to draw a second, adjacent line, creating two parallel, unmerged stripes. After 30 minutes of incubation to allow initial cell settling, 11×10^6 DiO-labeled NIH-3T3 cells were resuspended in 3 mL of culture medium and added to fill the remaining space within the mold. The construct was incubated for 24 hours at 37 °C and 5% CO_2. Fluorescence imaging was performed using a ChemiDoc system to assess the integrity of the patterned lines and the overall sheet structure.

For marbled patterning, a circular PLA insert with four wavy partitions (600 μm wall thickness) was 3D printed to divide a 2 cm diameter circular PDMS mold into four separate regions. Each region was filled with 200 μL of DiO- or DiL-labeled NIH-3T3 cells, alternating between labels, with a total of 2.5×10^6 cells per region (Fig. S1e). After 15 minutes of incubation to allow initial cell settling, the insert was carefully removed. After 2 h of incubation, 1 ml of additional culture medium was added to the mold, and the construct was incubated for 24 hours at 37 °C and 5% CO_2. The integrity and preservation of the marbled pattern within the cell sheet were then evaluated using ChemiDoc fluorescence imaging.

Formation of perivascular cell sheet

To make perivascular cell sheets, GFP-labeled NIH-3T3 were co-cultured with RFP-labeled HUVECs. These cells were grown in their proper culture medium up to 90% confluency and then trypsinized and resuspend in a 1:4 ratio of HUVECs to gfp-3t3 in fibroblast growth medium (first strategy). The mixture was then poured into the 1 cm diameter PDMS mold and kept incubated at 37 °C and 5% CO_2 for up to 4 days and the media was refreshed every day. The microstructure evolution of the construct was monitored during the culture period using Zeiss inverted fluorescent microscopy using proper filters of FITC and TEXRED to visualize fibroblasts and HUVECs, respectively. As the second strategy, a bilayered prevascularized cell sheet was fabricated by sequential seeding of cells. First, 1.5×10^6 GFP-labeled NIH-3T3 were seeded into a 1 cm PDMS mold and incubated for 2.5 hours. Next, 1.5×10^6 RFP-labeled HUVECs were gently added on top of the fibroblast layer to minimize disruption. Followed by 1 day of incubation, fluorescent imaging were performed to monitor the integration of HUVECs in the co-culture.

Microstructure evaluation

Microstructure and cellular distribution in cell sheets were assessed using fluorescence staining, live/dead viability assays, and histological analysis. Alexa Fluor™ 488 Phalloidin, DAPI (4′,6-diamidino-2-phenylindole), and a Viability/Cytotoxicity Kit (Cat #: L3224, Thermo Fisher Scientific) were used for fluorescence-based assessments, while hematoxylin and eosin (H&E) and Picrosirius Red (PSR) stains were used for histological evaluation.

For fluorescence staining, we followed the same protocol reported previously.[31] Briefly, NIH-3T3 cell sheets were fixed 1 day after formation using 4% paraformaldehyde at room temperature for 1 hour, followed by three washes with phosphate-buffered saline (PBS). A staining solution was prepared by diluting Alexa Fluor™ 488 Phalloidin stock solution (300 units in 1.5 mL methanol) and DAPI stock solution (10 mg mL^{-1} in deionized water) in 0.1% Triton X-100 in PBS, at final dilution ratios of 1 : 1000 and 1 : 2000, respectively. A total of 500 μL of staining solution was added to each sample and incubated for 1 hour at room temperature. High-magnification imaging was performed using an upright confocal microscope (Nikon A1R), and low-magnification fluorescent images were captured using an inverted microscope (Nikon Ti2) using proper filters of DAPI and FITC.

For live/dead staining, NIH-3T3 cell sheets were stained 1 day after formation using the Viability/Cytotoxicity Kit. Calcein-AM and ethidium homodimer were diluted in fibroblast growth medium at ratios of 1 : 2000 and 1 : 500, respectively. A 500 μL volume of the staining solution was added to each sample, followed by incubation at 37 °C for 30 minutes. After washing with PBS, fluorescent images were captured using an inverted microscope (Olympus IX51) using proper filters of FITC and Texas Red filters.

For histological evaluation, fixed cell sheets were dehydrated, embedded in paraffin, and sectioned to obtain cross-sectional views. Staining was performed using H&E and Picrosirius Red protocols, and images were acquired using an inverted microscope with appropriate filters (EVOS, Thermo Fisher Scientific).

Cellular behavior assessment

The behavior of NIH-3T3 fibroblasts in conventional 2D culture and in self-assembled 3D cell sheet formats was evaluated using Alamar Blue assay (ABA, Cat#: DAL1025, Thermo Fisher Scientific) for mitochondrial metabolic activity, Pierce™ BCA Protein Assay (Cat#: A55864, Thermo Fisher Scientific) for total protein content, and 1-step quantitative reverse transcription PCR (qRT-PCR, Cells-to-CT™ 1-Step Power SYBR™ Green Kit, Cat#: A25601, Thermo Fisher Scientific) for gene expression analysis of β1-integrin and E-cadherin.

For the Alamar Blue assay, a 10% (v/v) ABA working solution was prepared in fibroblast growth medium. A volume of 500 μL of this solution was added to each sample and incubated in the dark at 37 °C for 90 minutes. Fluorescence intensity was measured using a plate reader (Tecan Infinite M200 Pro) at excitation/emission wavelengths of 560/590 nm. For each sample, three 100 μL aliquots were transferred to a 96-well plate and read in triplicate. The ABA solution alone was used as a negative control, and 2D cultured NIH-3T3 cells served as the positive control (n = 3).

Total protein content was measured using the BCA assay following enzymatic digestion of samples. Both 3D cell sheets and 2D controls were digested in 500 μL of 2 mg mL^{-1} collagenase/dispase (Sigma-Aldrich, Cat# 10269638001) in PBS for 2 hours at room temperature. Digested samples were mixed thoroughly and lysed with an equal volume of 0.5% (v/v) Triton X-100 in PBS for 15 minutes at room temperature. Then, 25 μL of each replicate was transferred to a 96-well plate and mixed with 200 μL of BCA working reagent (prepared at a 50 : 1 ratio of Reagent A : B). Plates were incubated at 37 °C for 30 minutes, cooled to room temperature, and absorbance was measured at 562 nm using the plate reader. Digestion and lysis solution alone served as the negative control, and 2D cultured cells were used as the positive control (n = 3, measured in triplicate).

For gene expression analysis, qRT-PCR was performed on single-layer 3D cell sheets and 2D cultured NIH-3T3 cells seeded at the same density using Cells-to-CT™ 1-step PowerSYBR® Green kit. Target genes included E-cadherin (cell–cell adhesion marker), β1-integrin (cell–ECM adhesion marker), and β-actin as the housekeeping gene (Table 1). Samples were first digested with 500 μL of 2 mg mL^{-1} collagenase/dispase for 2 hours at room temperature. Cells were counted and gently centrifuged to remove enzyme solution, resuspended in 50 μL of chilled PBS per 1×10^5 cells, then centrifuged again and resuspended in 5 μL chilled PBS per 1×10^5 cells. Five microliters of the resulting suspension was added to each well of a 96-well PCR plate (n = 3 per group). Cell lysis was performed by adding 50 μL of lysis solution (provided in the kit), followed by 5 minutes of incubation at room temperature. Then, 5 μL of stop solution (provided in the kit) was added to each well.

A master mix was prepared according to the kit instructions using gene-specific primers for a 20 μL reaction volume, including 2 μL of cell lysate per well. Reactions were run using a thermal cycler real-time PCR machine (Biorad T100), with three replicates per primer set and nuclease-free water as a no-template control (NTC). Relative gene expression was calculated using the ΔΔCt method, normalized to β-actin, using Bio-Rad CFX Manager software.

In vivo demonstration of cell sheet integration in wound

Porcine full-thickness burn model. A validated porcine full-thickness burn model was employed as previously described.[32] This pilot study was conducted with one female Yorkshire pig, selected for its anatomical and physiological skin similarity to human skin. The study protocol was approved by the McMaster University Animal Research Ethics

Table 1 Primers' sequence used for qPCR (5′ to 3′)

Target gene	Forward	Reverse
E-Cadherin	AACCCAAGCACGTATCAGGG	ACTGCTGGTCAGGATCGTTG
β1-Integrin	AATGTGTTCAGTGCAGAGC	TTGGGATGATGTCGGGAC
β-Actin	GGCTGTATTCCCCTCCATCG	CCAGTTGGTAACAATGCCATGT

Board (AREB) under AUP# 22-08-29 and conducted in accordance with institutional guidelines.

The animal was acclimatized in the facility for two weeks prior to the procedure. On the day of burn induction, the pig weighed 35 kg and had a dorsal length of 60 cm. Under general anesthesia (5% isoflurane in 100% O_2) and analgesia (subcutaneous 0.05 mg kg^{-1} buprenorphine, 0.2 mg kg^{-1} ketamine, and 0.5–1.0 mg atropine), multiple 5 × 5 cm full-thickness burns were created on the dorsal surface using a custom-designed aluminum block heated to 200 °C. A 3 cm gap was maintained between adjacent wounds. Post-operative analgesia included oral tramadol (2–4 mg kg^{-1} every 8 hours), administered according to veterinary guidance. Full-thickness excision of burned tissue was performed 48 hours post-burn, down to the muscle fascia, on day 0 (grafting day).

Sample preparation and grafting. In this pilot demonstration, human umbilical cord-derived mesenchymal stem cells (UC-MSCs) cell sheet were grafted onto a full-thickness thermal wound to investigate the integration of cell sheet to the wound site and monitoring its acceptance and wound healing process over 40 days of experiment. No treatment (burn alone) wound, served as the negative control to represent the natural course of healing without intervention.

UC-MSCs were selected for this pilot *in vivo* study based on their demonstrated wound healing capacity,[32] accessibility, and immunosuppressive properties.[33] Following the previously described protocol for cell sheet fabrication, approximately 30×10^6 UC-MSCs were suspended in 10 mL of growth medium and seeded into a sterile 5 cm diameter circular PDMS mold. After 5 hours of incubation at 37 °C and 5% CO_2, an approximate 3 cm diameter UC-MSC cell sheet was formed and designated as the test graft for transplantation. Live/dead assessment performed after 5 h and 1 day of UC-MSCs sheet formation to evaluate the viability of cells before grafting.

UC-MSCs sheet was rinsed three times with Ringer's buffer to remove excess culture medium prior to transplantation. The UC-MSC cell sheet adhered immediately to the wound site upon placement and did not require additional fixation.

Post-operative wound dressings were applied following a standard protocol. Each wound was covered with a paraffin-based non-adherent dressing, followed by wet-to-dry sterile gauze layers. Dressings were secured using an adhesive breathable film, a custom-fitted porcine jacket (Lomir Biomedical Inc.), and an elastic spandex tube (Weaver Leather, LLC). Dressing changes were performed two to three times per week at predetermined time points.

Animal health and wound status were monitored by veterinary staff, in accordance with institutional safety guidelines. The animal remained in stable condition throughout the study with no adverse events observed. On day 40, the pig was euthanized *via* intravenous injection of 100 mg kg^{-1} pentobarbital.

UC-MSC cell sheet adhesion to the wound - *in vivo* testing

Integration of cell sheet to the wound were monitored throughout the study during regular dressing changes. Gross images were captured at each timepoint using a mirrorless digital camera (Sony α7R II), and wound were examined for signs of infection, inflammation, or bleeding. On day 40, full-thickness tissue biopsies were collected from the center of each wound (negative control and UC-MSC cell sheet). Samples were processed using standard hematoxylin and eosin (H&E) histological protocol. Histological sections were imaged using ImageScope software.

Statistical analysis

All data are presented as mean ± standard deviation (SD). Statistical significance was determined using Student's *t*-test in Microsoft Excel, with a *p*-value less than 0.05 considered statistically significant.

Results and discussion

Cell sheet formation process

Adherent cells naturally tend to attach either to surrounding cells or to other suitable substrates.[34] Building on this principle, we developed a novel biofabrication technique to generate large-scale, free-standing cell sheets through a self-assembly process. This method leverages high-density cell seeding on flat, low-adhesion surfaces to promote extensive cell–cell interactions, resulting in planar cellular sheets (Fig. 1A). When cells are seeded at low densities on low surface energy substrates, they remain sparsely distributed, often forming localized spheroidal aggregates.[11] This is generally attributed to the predominance of cell–cell adhesion over cell-substrate adhesion in such environments.[35] Based on this principle, we chose pristine polydimethylsiloxane (PDMS) as our 3D culture vessel material due to its low surface energy, non-cell-adhesive properties, cost-effectiveness, ease of molding into defined shapes, high gas permeability, and mechanical stability for this fabrication method.[36,37]

Cell sheet formation begins by dispensing a cell suspension at a density sufficient to achieve near-confluent

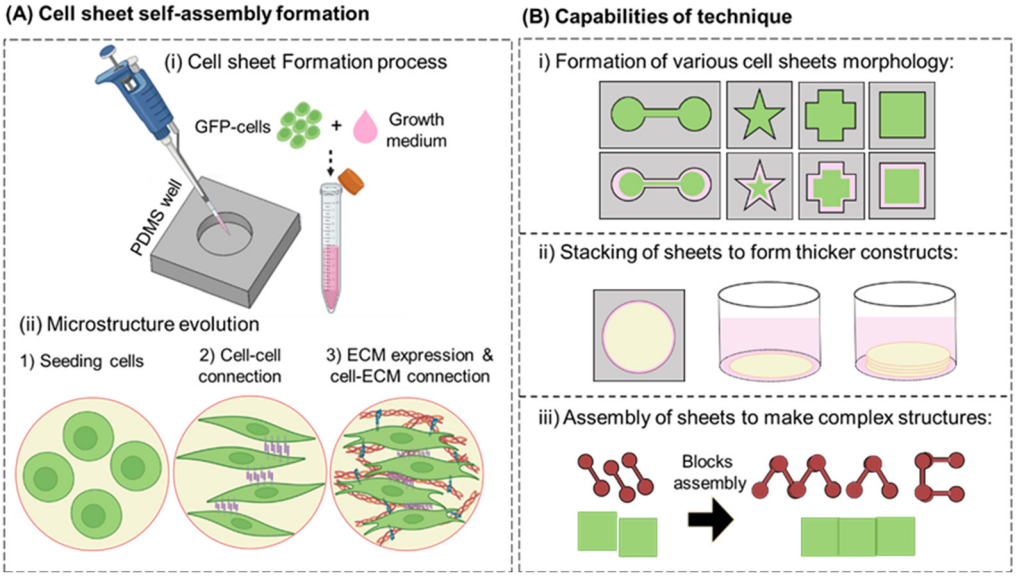

Fig. 1 Overview of the scaffold-free cell sheet biofabrication technique and its capabilities. (A) Schematic representation of the fabrication process: (i) cells at high density are seeded into untreated, non-adherent PDMS molds. (ii) cell sheet formation progresses through self-assembly, beginning with cell–cell junctions, followed by ECM deposition and cell–ECM interactions. (B) Versatility of the method: (i) generation of cell sheets in customizable shapes; (ii) stacking to form thicker tissue-like constructs; and (iii) modular assembly of building blocks into larger and more complex structures.

coverage of the PDMS well surface, followed by incubation at 37 °C with 5% CO_2 (Fig. 1A, i). Within approximately 15 minutes, cells settle to the bottom of the well by gravity and begin to self-organize, forming well-integrated, planar, cell sheet after a maximum of 1 day (Fig. 1A, ii). It is important to note that freshly prepared PDMS wells were used to fabricate the cell sheets in order to minimize the risk of protein absorption by the PDMS surface. Such absorption could occur due to the presence of serum proteins in the culture medium and ECM secreted by the cells themselves, potentially hindering proper 3D assembly.

However, because our technique rapidly promotes the self-assembly of cells into 3D sheets within only a few hours after seeding, the likelihood of significant protein absorption interfering with this process is very low. As shown in Fig. S2, nearly all the cells seeded into the PDMS well rapidly self-assembled into continuous cell sheet, with only a small fraction remained at the bottom of the well without integrating into the sheet. We also tested other low-adhesion substrates, including ultra-low attachment well plates (Corning, Cat# 3473), PDMS coated well plates, and liquid-phase silicone oil coated well plates. Across all conditions, critical-density seeding consistently led to cell sheet formation (Fig. S3), whereas conventional adherent culture plates promoted full substrate attachment and failed to support sheet formation.

These results, along with previous findings on spheroid self-assembly on non-adherent surfaces,[11] suggest that cell sheet formation relies on continuous cell–cell adhesion in the absence of substrate anchorage (Fig. 1A, ii), which is also further investigated in the next section (Fig. 2B). The resulting cell sheets are free-standing, cell-only tissue-like constructs, sufficiently robust to withstand gentle handling, such as transfer with tweezers or a spatula to larger containers for improved nutrient exchange. Their final shape is defined by the geometry of the PDMS mold, enabling the fabrication of various shapes (Fig. 1B, i).

Multilayered, and more complex constructs can also be generated by stacking individual sheets (Fig. 1B, ii) or overlapping their edges to create patterned tissue-like assemblies (Fig. 1B, iii).

Optimization of cell seeding density for sheet formation

To determine the critical cell seeding density required for the formation of well-integrated and mechanically robust cell sheets, we investigated the effects of varying cell concentrations in circular PDMS mold (diameter = 1 cm). For this purpose, NIH/3T3 fibroblasts were initially used. Cell suspensions ranging from 0.3×10^6 to 2×10^6 cells per well were seeded and incubated for 24 hours at 37 °C and 5% CO_2, after which the resulting structures were visually assessed using stereomicroscope (Fig. 2A).

At lower seeding densities (below 0.8×10^6 cells per well), cells formed dispersed spheroidal or multi-spheroidal aggregates, lacking large-scale structural integration. These aggregates did not develop into continuous sheets. In contrast, increasing the seeding density to $\geq 0.8 \times 10^6$ cells per well initiated the formation of contiguous, sheet-like structures (Fig. 2A). However, at intermediate densities ($0.8–1.0 \times 10^6$ cells per well), these sheets exhibited irregularities such as curling edges or self-folding, likely due to insufficient cell–cell cohesion or internal mechanical imbalance during the self-assembly process.[38]

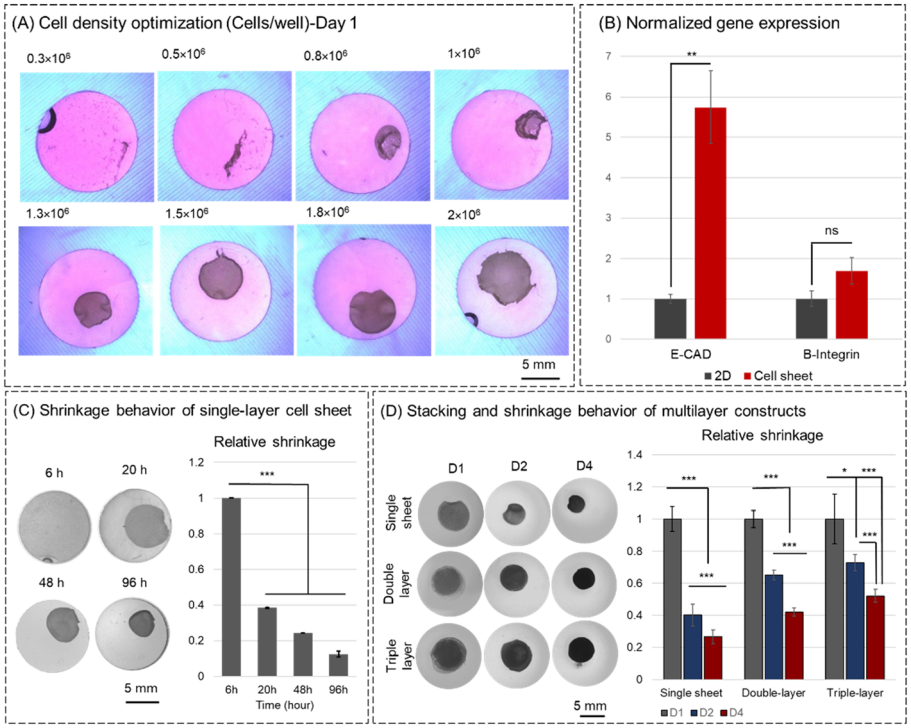

Fig. 2 Macrostructure optimization, gene expression of adhesion proteins, and contraction behavior of scaffold-free cell sheets. (A) Seeding density optimization in 1 cm diameter PDMS molds shows that densities $\geq 0.8 \times 10^6$ cells support sheet formation, with 1.5×10^6 cells identified as optimal for producing flat, well-integrated, and mechanically robust NIH/3T3 sheets. (B) RT-qPCR analysis of NIH/3T3 shows ~5.7-fold upregulation of E-cadherin in 3D cell sheets compared to 2D culture, indicating cell–cell adhesion as a key mechanism in early stages of self-assembly (day 1). β1-integrin levels remained comparable between groups. (C) Time-course analysis of single-layer NIH/3T3 sheets reveals ~60% contraction within the first day, followed by a slower rate of shrinkage over four days. (D) Comparison of single-layer and stacked (double- and triple-layer) NIH/3T3 constructs demonstrates that increased layering reduces the overall shrinkage, while all constructs maintain planar geometry (*, **, ***: $p < 0.05$, 0.01, and 0.001, respectively).

Densities above 1.3×10^6 cells per well consistently yielded well-defined, circular sheets that remained planar, intact, and detached from the PDMS substrate. These constructs displayed sufficient mechanical integrity to be handled without structural damage. Based on geometric estimations, a minimum of ~1.3×10^6 trypsinized NIH/3T3 cells is required to fully cover a 1 cm diameter area.

Our results suggest that a critical threshold, approximately 70% of this theoretical density, is necessary to initiate cohesive sheet formation. For NIH/3T3 fibroblasts, we identified 1.5×10^6 cells per mold (~1.9×10^6 cells per cm^2) as the optimal seeding density, providing the best balance between sheet integrity, mechanical robustness, and reproducibility.

Although the precise mechanism by which cell density influences the self-assembly of cells into planar and cohesive sheets in this platform requires further investigation, previous spheroid self-assembly studies suggest that cell–cell contacts play a major role.[11] To further explore this underlying mechanism, we next evaluated the expression of adhesion molecules under the optimized cell seeding condition.

Gene expression of adhesion proteins

To investigate the molecular basis of cellular self-assembly in 3D cell sheets, we analyzed the gene expression of adhesion-related proteins using qRT-PCR after 1 day of NIH/3T3 cell sheet formation and compare it to conventional 2D culture. Specifically, we examined the expression of E-cadherin, a key mediator of cell–cell adhesion, and β-integrin, involved in cell–ECM and cell–substrate interactions.[39,40] As the results show (Fig. 2B), E-cadherin expression was found to be 5.7-fold higher in the 3D cell sheet samples compared to 2D monolayers, indicating a pronounced upregulation of cell–cell junction formation during the early stages of self-assembly process. This result provides strong molecular-level evidence supporting our earlier notion that cell–cell adhesion drives the formation of planar sheet-like structures in non-adherent PDMS molds. Moreover, β-integrin expression in 3D cell sheets was slightly elevated compared to 2D cultures, though the difference was not statistically significant. As PDMS does not support cell–substrate adhesion, the observed β-integrin expression likely reflects early cell–ECM interactions with the matrix produced by the cells as early as day 1, a topic explored further in subsequent sections (Fig. 5E). Notably, our results indicate that, while these interactions are beginning to form, cell–cell adhesion remains the dominant mechanism during the initial stages of cell sheet formation.

Taken together, these findings suggest a two-phase model of self-assembly: initial organization is governed primarily by cell–cell adhesion, followed by the gradual emergence of

ECM-mediated stabilization. This process is thought to contribute to the mechanical stability and maintenance of the planar architecture of the sheets. Furthermore, the gene expression results, along with the observation of sheet formation at a critical cell density, indicate that at or above this density, the equilibrium of traction forces within the constructs primarily supports sheet structure formation and maintenance over the experimental timeframe. In contrast, at lower cell densities, where gaps form among cells across different regions, cells attach to neighboring cells, and traction forces lead to the formation of dispersed cellular aggregates within the PDMS wells.

Contraction behavior of cell sheets

To evaluate the ability of self-assembled cell sheets to maintain their flat morphology over time, we monitored their contraction behavior over a 4-day culture period. Single-layer cell sheets were formed by seeding 1.5×10^6 NIH/3T3 fibroblasts into 1 cm-diameter circular PDMS molds, and images were taken at 6, 20, 48, and 96 hours. A mechanically robust sheet formed within approximately 6 hours post-seeding at this density. However, significant contraction occurred during the first 24 hours, with the diameter shrinking by 61.57 ± 3.9% (Fig. 2C). The rate of contraction slowed over time, with a further 59.92 ± 1.44% reduction (relative to day 1) by day 2, and 33.8 ± 0.89% by day 4 (relative to day 2), indicating that the strongest contractile forces are exerted early in the culture period.

Layering and stacking of cell sheets are of interest because they enable the formation of more physiologically relevant thick tissue constructs with high cellular density, without the use of external scaffolding materials, thereby better resembling the cell density of native tissues while allowing the cells to produce their own ECM microenvironment suitable for functionality. To investigate how stacking and increased thickness influence contraction, multilayered constructs were created by stacking cell sheets.[41] For this experiment, individual sheets were first cultured for 1 day to allow initial compaction. On day 1, sheets were gently stacked to form double- and triple-layer constructs and returned to culture. Images were taken immediately after stacking (D1), one day post-stacking (D2), and three days post-stacking (D4), and the contraction behavior was compared across single-, double-, and triple-layer constructs (Fig. 2D). At D2 (one day post-stacking), single-layer sheets contracted by 59.92 ± 6.59%, whereas double- and triple-layered sheets contracted by 34.80 ± 3.04% and 27.25 ± 5.09%, respectively. By D4, this trend persisted, with single-layer sheets showing the highest contraction relative to D1 (73.48 ± 4.31%), followed by double layers (58.09 ± 2.70%) and triple layers (47.95 ± 4.06%).

Remarkably, our fabrication method enables the formation of NIH/3T3 fibroblast cell sheets within just 6 hours of seeding, significantly faster than conventional techniques, which typically require several days to weeks.[42] This rapid assembly occurs in non-adherent PDMS wells, where cells self-organize through cell–cell adhesion. As intercellular connections strengthen, collective traction forces, driven by actomyosin-generated tension, pull the sheet inward, leading to substantial compaction within the first 24 hours while maintaining a planar architecture.[43] This contraction is most pronounced on the first day and gradually decreases, likely due to extracellular matrix (ECM) deposition and the emergence of stabilizing cell–ECM interactions.[44] Additionally, when cell sheets are stacked, the high cell density and ECM components of the individual sheets promote interlayer adhesion. This interlayer bonding helps counteract traction forces within the stacked sheets, leading to reduced contraction and improved shape retention in the multilayered constructs.[14]

Versatility of the cell sheet biofabrication technique

To evaluate the versatility of the developed cell sheet biofabrication method, we assessed its applicability across different adherent cell types, its scalability for generating sheets of various sizes, and its capacity to form geometrically diverse sheet morphologies. These evaluations aimed to determine whether the technique could be adapted for broader applications in tissue engineering, regenerative medicine, and biofabrication.

Compatibility with various cell types

Multiple adherent cell types were seeded into 1 cm diameter circular PDMS molds and incubated for 1 day. The optimized seeding density for each cell type is summarized in Table S1. As shown in Fig. 3A, robust and continuous self-assembled cell sheets were successfully formed using a variety of cells, including primary human skeletal muscle cells (HSKMCs), mouse myoblasts (C2C12), mouse preadipocytes (3T3-L1), human cytotrophoblast placenta cells (BeWo), human osteoblast-like Saos-2 cells, normal human skin fibroblasts (NF), human burn-derived mesenchymal stem cells (BD-MSCs), and human umbilical cord-derived mesenchymal stem cells (UC-MSCs). All of these cell types exhibited self-assembly behavior, forming homogenous and structurally stable planar constructs. It is worth noting that each cell type exhibited different contraction behaviour. Some cells, such as NF, Opo-Moo-M17, and BD-MSC, led to the formation of cell sheets comparable in size to the NIH/3T3 sheet, while others showed less shrinkage after one day of formation (Fig. S4). This difference may be due to variations in the strength of cell–cell connections, as well as the extent of ECM deposition by each cell type, which could potentially alter the force balance toward the centre of the cell sheet and influence its shrinkage behaviour.[14] Moreover, other studies have reported that various cell types express distinct levels of intercellular adhesion molecules and display different orientations of their cytoskeletal actin filament networks.[45] Such variations are likely to contribute to differences in contraction behaviour among cell types. A more detailed characterization

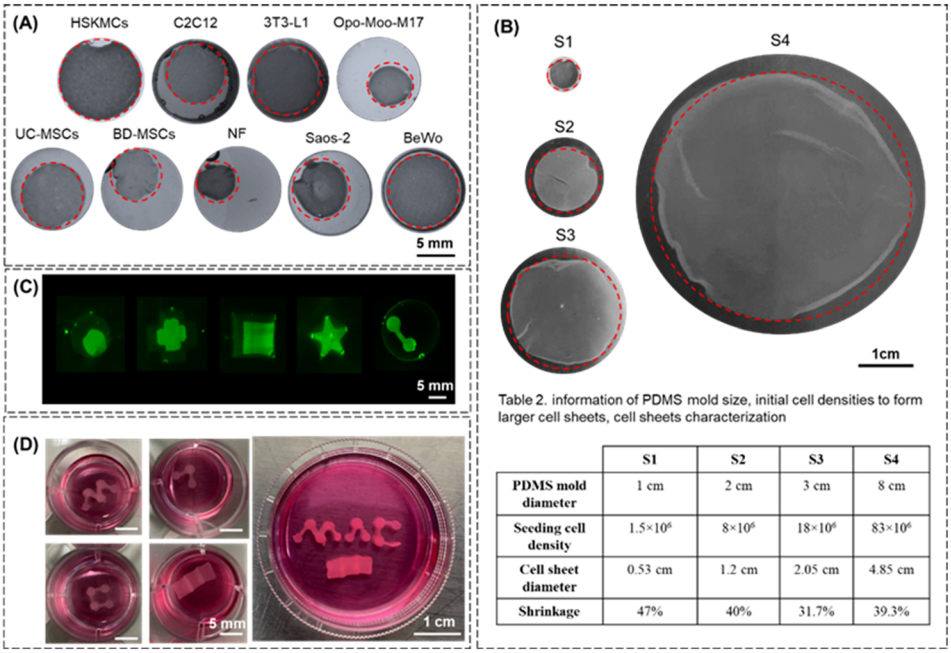

Table 2. information of PDMS mold size, initial cell densities to form larger cell sheets, cell sheets characterization

	S1	S2	S3	S4
PDMS mold diameter	1 cm	2 cm	3 cm	8 cm
Seeding cell density	1.5×10^6	8×10^6	18×10^6	83×10^6
Cell sheet diameter	0.53 cm	1.2 cm	2.05 cm	4.85 cm
Shrinkage	47%	40%	31.7%	39.3%

Fig. 3 Versatility of the developed scaffold-free cell sheet biofabrication technique. (A) Cell sheets successfully generated from various primary cells, cell lines, and stem cells. (B) Scalable fabrication of large-area circular NIH/3T3 sheets ranging from ~0.5 cm to ~5 cm in diameter. (C) Customizable NIH/3T3 sheet morphologies achieved using PDMS molds with different shapes. (D) Modular assembly of individual NIH/3T3 cell sheets into complex structures for advanced tissue modeling.

of shrinkage profiles and the molecular and structural mechanisms underlying them is therefore needed.

In contrast, certain cell lines, such as human umbilical vein endothelial cells (HUVECs) and primary human corneal epithelial cells (HCECs), did not form continuous sheet structures under identical conditions (Fig. S5). This observation may suggest limited cell–cell adhesion or an alternative self-assembly behavior in these cell types rather than continuous sheet-like assembly.[46] To the best of our knowledge, vascular endothelial cells have mainly been reported in co-culture with supporting cells such as MSCs and fibroblasts to promote vascularization within cell sheets,[17] while the formation of a continuous cell sheet composed solely of vascular endothelial cells has not yet been demonstrated.

On the other hand, Hung *et al.* have shown that corneal epithelial cells can form continuous planar cell sheets when cultured at the interface of an aqueous biphasic system.[47] Based on this, it can be inferred that differences between the PDMS mold used in this study and the aqueous interface, such as substrate stiffness, may play a critical role in promoting cellular self-assembly and the formation of well-integrated corneal epithelial cell sheets. To further assess this, future studies could explore culture vessels with varying stiffness, for instance by adjusting the PDMS to curing agent ratio, to optimize conditions for the self-assembly of HCECs.

Nonetheless, compared to most existing cell sheet biofabrication methods, our developed technique demonstrates the ability to rapidly form cell sheets; 6 hours for 3T3 fibroblasts and maximum of 24 hours for all other compatible cell types, a broader range of compatible cell types, including the successful formation of BeWo cell sheets, which are valuable for placental barrier *in vitro* studies. For example, the pH-induced cell sheet fabrication approach has been shown to be limited to fusing cells such as myoblasts. However, it could not effectively be used to form cell sheets with BeWo cells, despite their fusion potential.[14]

Additionally, other techniques that rely on external signals, such as light or electrical stimulation, have not yet demonstrated compatibility with a wide range of cell types.[24] Although temperature-responsive culture surfaces have supported the formation of cell sheets from various cell types, they present significant limitations, including high costs, and uncertainties regarding the impact of temperature shock on cellular function.[42] Furthermore, current cell sheet fabrication methods typically require prolonged culture periods, as they depend on the gradual development of cell–cell connections and conventional 2D ECM formation and deposition, which take time to develop sufficient mechanical stability for delamination and are less biomimetic compared to ECM structures formed directly in a 3D configuration.[30,42]

In contrast, our technique enables the rapid formation of 3D ECM structures by facilitating cell sheet development directly in a 3D format. Utilizing pristine PDMS, our method offers a simple, adaptable approach that does not require expensive equipment or external cues that could potentially harm cellular function or ECM delicate structure. These advancements effectively addresses the major limitations of existing fabrication techniques and significantly enhances the potential of our approach for diverse applications, including the development of

biological barrier models (*e.g.*, placental tissue) and implantable tissue grafts (*e.g.*, skin substitutes).

Scalability of technique

To assess the scalability of the fabrication process, NIH/3T3 cell sheets of varying diameters (ranging from ~0.5 cm to 5 cm) were generated by adjusting PDMS mold sizes and cell seeding density. All sheets were cultured for 1 day and demonstrated successful self-assembly and handling properties (Fig. 3B). **Table 2** summarizes the cell density, sheet diameter, and percentage shrinkage for each construct. Larger sheets retained sufficient mechanical robustness to be lifted using tweezers or spatulas after 1 day of culture, confirming that our technique supports the rapid production of handling-stable, large-area constructs (Fig. 3B).

The fabrication of large-area cell sheets remains challenging with many existing methods. For example, in aqueous biphasic systems[15] and delamination-based approaches,[24] scaling up the sheet size is hindered by interface instability and difficulties in maintaining uniform environmental conditions, often compromising sheet integrity at larger scales. Other techniques, such as the cellular self-assembly method reported by Larouche *et al.*, successfully produced fibroblast sheets measuring approximately 6 × 9 cm on adherent culture plates; however, the process required approximately 17–31 days to complete.[48] Although their method yielded well-integrated, large-scale sheets, the prolonged culture duration represents a significant limitation. In this study, we demonstrated that our technique enables the rapid fabrication of large-area, mechanically stable, and robust cell sheets. This capability is particularly advantageous for biomedical applications such as wound coverage and tissue grafting, where large sheets are urgently required for acute injuries, as well as for emerging fields such as cultivated meat production, where the engineering of full-sized meat constructs is necessary.

Geometrical customization and modular assembly

To explore the geometrical flexibility of the technique, PDMS molds of various geometries, including square, cross, dumbbell, and star shapes, were fabricated and seeded with GFP-positive NIH/3T3 cells. As shown in Fig. 3C, the resulting cell sheets maintained the geometry of their original molds even after shrinkage during self-assembly. This shows that contraction forces act uniformly toward the sheet center,[14] preserving the initial shape of the mold. The individual cell sheets produced are inherently adhesive and can bind to other cell sheets or naturally produced ECM components. Building on this characteristic, we further demonstrated the modular assembly capability of the sheets. Using tweezers, dumbbell-shaped sheets were aligned and overlaid at their ends to form a custom macrostructure spelling the letters "MAC". After 1 day of incubation, the assembled construct remained monolithic and mechanically stable, as shown in Fig. 3D, and could be manipulated multiple times without disintegration.

This modular, "LEGO-like" approach demonstrates the potential to construct complex, large-scale 3D structures by assembling multiple sheets or by wrapping them around sacrificial cores. To the best of our knowledge, this is the first demonstration of such capability within cell sheet biofabrication techniques. This limitation in previous methods likely stems from the reliance of most fabrication strategies on 2D cell culture followed by a delamination step,[42] which restricts the final shape and size of the sheets to the dimensions of standard culture plates, typically resulting in simple circular or rectangular formats. In contrast, the use of PDMS molds as culture vessels in this study enabled the fabrication of sheets in a wide range of sizes and more intricate geometries, with modular assembly allowing the construction of more complex and irregular structures. Such strategies may also benefit *in vivo* grafting, particularly for covering irregular or difficult-to-access surfaces, such as wound sites between fingers, where continuous graft application is challenging. In these cases, cell sheets of desired size and shape could be modularly assembled directly at the wound site to achieve efficient coverage.

Cell sheet patterning and coculture strategies

To evaluate the ability of the developed cell sheet biofabrication method to mimic physiologically relevant multicellular environments, we investigated its suitability for co-culturing and spatial patterning of different cell populations within a single construct. Accurately modeling *in vivo* tissue conditions requires consideration of the symbiotic interactions among multiple cell types within a given tissue, as well as the interplay between that tissue and surrounding systems such as the vascular and nervous networks.[30] These cellular and inter-tissue interactions play a critical role in regulating tissue function, development, and regeneration.[12] To assess whether our technique can support such complexity, we developed and tested a series of co-culture and patterning strategies aimed at reproducing key features of native tissue architecture.

Bilayer and mixed co-culture systems

Two strategies were employed to demonstrate co-culture feasibility: sequential bilayering and simultaneous mixing. In the bilayer approach, DiL-stained NIH/3T3 cells (red) were first seeded into 1 cm diameter PDMS molds and incubated for 30 minutes at 37 °C with 5% CO_2 to allow them to settle and form an initial layer (Fig. S1a). After carefully removing the excess medium, DiO-stained NIH/3T3 cells (green) were gently introduced to form the second layer atop the first. After 1 day of incubation, the resulting cell sheet displayed two distinct but continuous layers of cells, as shown in Fig. 4A, i, confirming that the initial layer forms a stable base within 30 minutes and is not disrupted by subsequent cell addition.

In the mixed co-culture setup, DiO- and DiL-labeled cells were combined in a 1 : 1 ratio (0.75×10^6 each) and co-seeded simultaneously. After 1 day of incubation, the resulting sheet (Fig. 4A, ii) showed a homogeneous distribution of both cell types throughout the structure. Both cross-sectional and top view imaging revealed that, unlike the bilayer system, the mixed co-culture did not exhibit stratification but instead formed an interspersed distribution of both labeled cells. These results demonstrate that the technique enables both stratified and homogeneously mixed co-culture configurations, which could be tailored depending on the desired tissue architecture.

Patterned co-cultures using spatial confinement

To create spatially distinct cell regions within a single sheet, two mold-based patterning strategies were developed. First, a dumbbell-shaped PDMS mold with two cylindrical compartments connected by a narrow neck was used to limit cell suspension flow between compartments. DiO- and DiL-stained NIH/3T3 fibroblasts were seeded into each compartment at 15-minute intervals (Fig. S1b). Due to surface tension and mold geometry, cell suspension remained confined within their respective regions and let the cells loaded to each region to settle down and make connections with the adjacent region. After 1 day, a continuous but distinctly patterned cell sheet was formed, with a clear border between the two zones (Fig. 4A, iii).

In a second strategy, a temporary physical insert was 3D-printed from PLA to divide a circular PDMS well into two equal halves (Fig. S1c). DiO- and DiL-stained cell suspensions were seeded simultaneously into each side. After 15 minutes of settling, the insert was carefully removed, allowing the cells on each side to interact. By day 1, the two regions had formed an integrated sheet with a clearly visible boundary (Fig. 4A, iv), likely aided by gentle fluid movement during insert removal, which enabled minimal crossover and facilitated cell–cell interactions at the interface.

Freehand and marbling patterning

To demonstrate further versatility, we tested free-hand patterning using pipetting techniques (Fig. S1d). DiL-labeled cells were deposited in linear patterns using a fine pipette tip, allowed to settle for 15 minutes, and then DiO-labeled NIH-3T3 cells were added to fill the remaining space. After 1 day of culture, the resulting sheet preserved the hand-drawn pattern embedded within the larger construct (Fig. 4A, v1). Additionally, a 3D-printed insert with wavy partitions was used to create marbled patterns (Fig. S1e). Labeled cells (DiL and DiO) were seeded into alternating compartments of the mold, and the insert was removed after 15 minutes of incubation. The resulting sheet maintained the wavy marbled pattern after 1 day (Fig. 4A, v2).

These patterning strategies demonstrate that the self-assembly process in this method can support the spatial

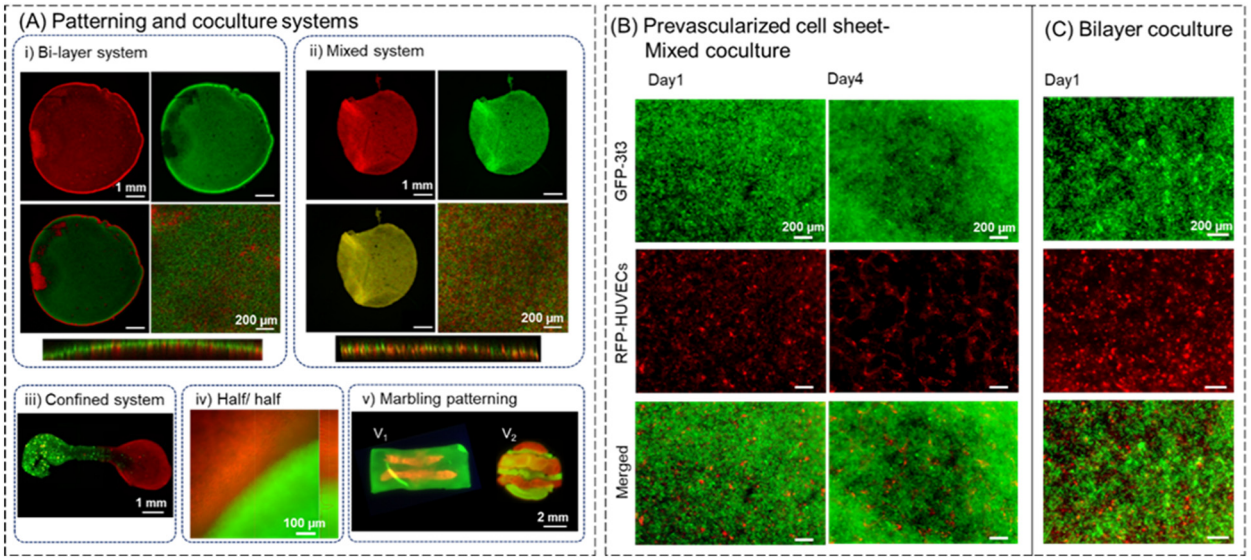

Fig. 4 Patterning and co-culturing strategies within self-assembled cell sheet constructs. (A) Fluorescent micrographs demonstrate five distinct patterning approaches: (i) bilayer patterning achieved through sequential deposition of DiL- and DiO-labeled NIH/3T3 cells, forming two distinct yet integrated layers within a single construct. (ii) Mixed co-culture strategy enabling homogeneous distribution of heterogeneous DiL- and DiO-labeled NIH/3T3 cells throughout the sheet. (iii) Constrained patterning using a dumbbell-shape PDMS mold, where sequential cell seeding of DiL- and DiO-labeled NIH/3T3 cells into regions maintains spatial patterning. (iv) Half-and-half co-culture using an external PLA insert to divide the mold into two compartments; following 15 min of cell settling, the insert is removed to allow sheet fusion at the interface. (v) Marbling patterns generated *via* v1) freehand pipetting of labeled NIH/3T3 cells and v2) use of a wavy-patterned PLA insert to spatially organize distinct labeled NIH/3T3 cells cell populations. (B) Mixed co-culture of GFP-NIH/3T3 fibroblasts and RFP-HUVECs promotes vascular-like network formation after 4 days, demonstrating potential for prevascularized constructs. (C) Bilayer co-culture of fibroblasts (bottom layer) and HUVECs (top layer) creates a prevascularized sheet *via* sequential deposition.

organization of multiple cell types, enabling the fabrication of structured, heterogeneous 3D cell sheets. By mimicking the native tissue micro- and macrostructure through tailored co-culture and patterning approaches, such as layered arrangements (*e.g.*, retina), mixed co-culture (*e.g.*, vascularized dermis), spatially distinct compartments (*e.g.*, muscle–tendon junction), and marbling patterns (*e.g.*, muscle–fat), this approach supports the fabrication of complex tissue constructs in a physiologically relevant configuration. Furthermore, the single-step nature of this method enhances its feasibility and adaptability compared to other fabrication techniques, which often require multistep surface modifications or post-processing tools for cell patterning.[49] This capability is particularly valuable for applications such as *in vitro* tissue modeling, and spatially guided cell therapies, where precise control over multicellular architecture is essential.

Pre-vascularization of cell sheets

A major challenge in engineering thick tissue constructs (>200 μm) is the absence of sufficient vascular networks, which can lead to necrotic core formation due to limited diffusion of oxygen and nutrients.[17] Since our technique enables stacking multiple cell sheets to form thicker tissue-like constructs, we investigated fabricating pre-vascularized sheets to address the possible challenge of necrotic core formation in these thicker constructs. Given prior evidence that endothelial cells are supported *in vivo* by surrounding stromal cells such as fibroblasts, pericytes, and vascular smooth muscle cells, which provide ECM components and biochemical signals essential for vascular organization and maintenance,[50] two co-culture strategies were selected to facilitate vascular-like network formation within fibroblast sheets due to their potential to generate prevascularized tissue models. Previous studies used NIH/3T3 fibroblasts in coculture with HUVECs and showed support for vasculature formation.[51,52] Accordingly, we used them to demonstrate vascularization using our cell sheet biofabrication technique. To achieve a fully humanized vascular sheet, we also cocultured NFs with HUVECs, which likewise resulted in vasculature formation (Fig. S7).

In the first strategy, RFP-labeled HUVECs were mixed with GFP-labeled NIH/3T3 fibroblasts at a 1 : 4 ratio in fibroblast growth medium, and the suspension was introduced into PDMS molds. The samples were incubated for 4 days, during which microstructural changes were monitored. As shown in Fig. 4B, HUVECs formed microvascular-like networks within the fibroblast-based cell sheet after 4 days of coculture. This result suggests that the presence of fibroblasts supports HUVECs organization and assembly, likely by providing a collagenous ECM substrate and secretion of growth factors that facilitates adhesion and directed migration.[46]

In the second strategy, a bilayered prevascularized fibroblast cell sheet was fabricated by sequentially seeding HUVECs on top of NIH/3T3 cells. Fluorescent imaging confirmed the integration of HUVECs atop the fibroblast layer, resulting in a cohesive bilayer construct (Fig. 4C). This configuration allowed HUVECs to assemble within a fibroblast-supported microenvironment, forming a unified prevascularized cell sheet. Stacking multiple layers of these constructs can enable the development of interconnected vascular networks, potentially mitigating necrotic core formation in thicker tissue constructs.[53]

These findings suggest that, in the mixed co-culture platform, direct interaction between fibroblasts and endothelial cells supports the formation of interconnected vascular-like structures. In contrast, the bilayer co-culture strategy enables layer-by-layer integration of endothelial cells within thicker constructs, potentially facilitating vascular sprouting across layers and promoting angiogenesis throughout the tissue. Taken together, the results demonstrate that co-culture of HUVECs with fibroblasts supports the development of organized vasculature within a structurally stable cell sheet. Compared to other methods that rely on synthetic scaffolds or 2D surfaces,[54,55] this approach enables 3D, scaffold-free vascular-like network formation through self-assembly, more closely mimicking the physiological microenvironment of native tissues.

Microstructure evaluation of cell sheets

To investigate how the self-assembly process influences the microstructure, viability, and functionality of the resulting cell sheets, we conducted a series of fluorescent and histological staining assays. These evaluations aimed to characterize cell distribution, cytoskeletal organization, adhesion behavior, and ECM production during both early and extended culture periods. For these characterizations, NIH/3T3 fibroblasts were selected due to their central role in connective tissue maintenance. Fibroblasts are primary producers of ECM components, which provide essential structural, biophysical, and biochemical cues, and regulate the secretion of signaling molecules such as cytokines and growth factors.[56] Their key functions in tissue homeostasis and repair make fibroblasts particularly relevant for studying ECM formation and cell-matrix interactions. Furthermore, fibroblasts are widely used in *in vitro* tissue modeling and *in vivo* grafting applications, making them an ideal model for evaluating the potential of the fabricated cell sheets to replicate native tissue microenvironments.

Morphology, viability, and early assembly dynamics

To assess cellular morphology in the sheet format, 1.5×10^6 GFP-expressing NIH/3T3 cells were seeded into circular PDMS molds and cultured for 24 hours. Fluorescence imaging (Fig. 5A) showed tightly packed cells with cell–cell interactions, forming an integrated sheet-like structure. To evaluate the viability of cells within the construct, Live/

dead staining was performed on NIH/3T3 cell sheets after one day of formation. As shown in Fig. 5A, the majority of cells were viable, with only a few dead cells detected, indicating that the self-assembly process does not adversely affect cell survival.

To monitor the dynamics of cell–cell adhesion and the formation of cell sheet over time, GFP-positive NIH/3T3 cells were seeded at 1.5×10^6 cells per well and imaged *via* fluorescence microscopy at 1, 3, 5, and 20 hours post-seeding. As shown in Fig. 5B, cells had settled by 1 hour but remained loosely distributed with visible voids. By 3 hours, these gaps had narrowed, and cells began forming visible connections. At 5 hours, an increasingly interconnected structure formed, with enough mechanical integrity to allow for removal from the PDMS mold. By 20 hours, the void spaces were negligible, consistent with significantly enhanced cell–cell connection and compaction.

These results provide microscopic visual confirmation of the establishment and progressive strengthening of cell–cell interactions necessary for the formation of continuous, planar sheets. For deeper insight into cellular micro-organization, Phalloidin (F-actin) and DAPI (nuclei) staining were conducted on NIH/3T3 cell sheets cultured under the same conditions. The results (Fig. 5C) revealed a densely packed microstructure ($\sim 5.52 \times 10^5$ cells per cm^2) with homogeneously distributed nuclei and a well-developed actin cytoskeletal network. This interconnected randomly oriented cytoskeletal architecture likely contributes to the mechanical robustness and contractile behavior previously observed in the cell sheets.[57]

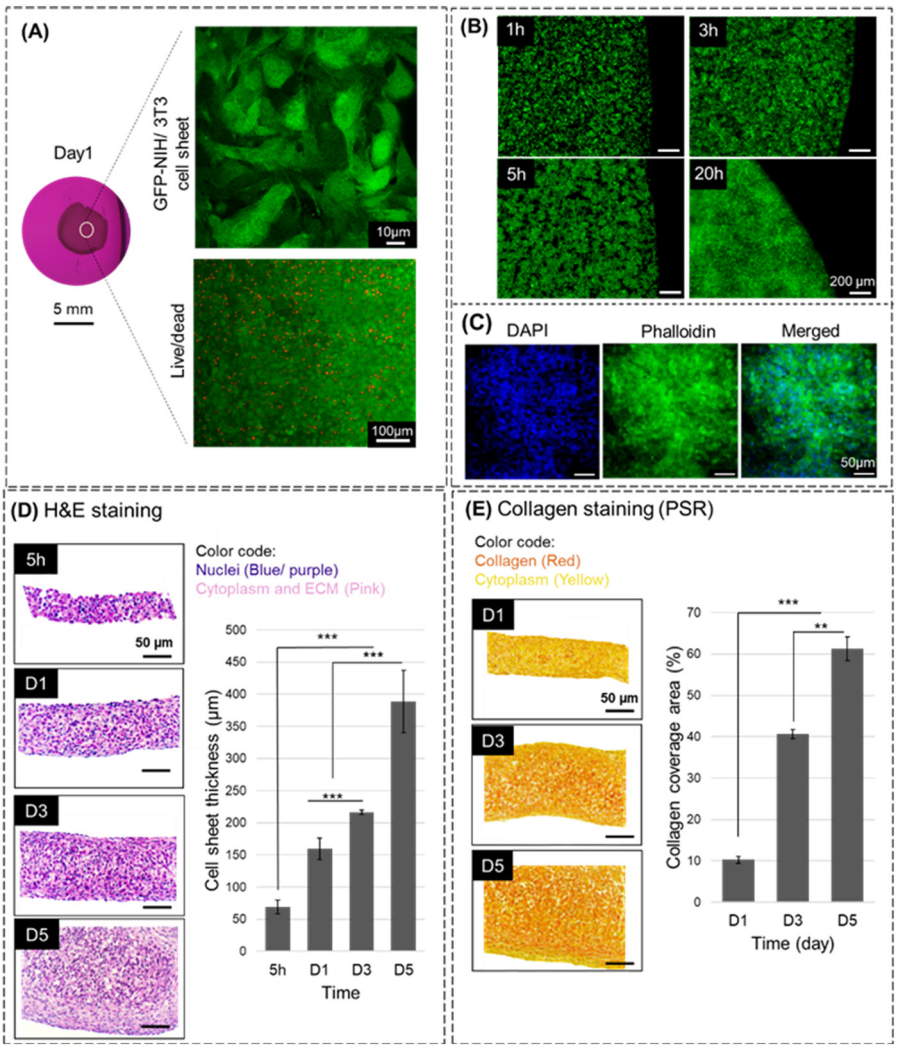

Fig. 5 Microstructural evaluation of self-assembled cell sheets. (A) Confocal micrograph of GFP-expressing NIH/3T3 cells after 1 day of sheet formation shows densely packed cells with suggesting the formation of cell–cell interactions; live/dead staining confirms high viability with minimal dead cells. (B) Time-lapse fluorescent imaging illustrates the progressive formation of intercellular junctions during the early stages of sheet assembly. (C) Phalloidin (F-actin cytoskeleton) and DAPI (nuclei) staining after 1 day confirms a densely populated structure with close-contact cytoskeletal networks. (D) H&E-stained cross-sections reveal multilayered cellular architecture with increasing sheet thickness over time, correlating with observed contraction behavior. (E) Picrosirius Red staining demonstrates progressive collagen deposition over 5 days, indicating active ECM production by NIH/3T3 fibroblasts. (**, ***: $p < 0.01$ and <0.001, respectively).

Structural evolution

To characterize internal structural changes over time, cross-sections of H&E-stained single-layer sheets were imaged after 5 hours, and 1, 3, and 5 days of culture (Fig. 5D). Notably, within only ~5 hours, the constructs reached ~10^9 cells per mL cellular density that is comparable to cell sheets produced by established fabrication techniques (~10^8–10^9 cells per mL).[14,18–20] At this early time point, a ~70 μm-thick planar structure had already formed, consisting of 5–6 cell layers. These values place our constructs at the upper end of the cellular densities reported for native tissue subunits (~10^8–10^9 cells per mL), highlighting the rapid and efficient nature of this method.

Consistent with observed macroscopic shrinkage, sheet thickness increased progressively, reaching ~160 μm on day 1, ~217 μm on day 3, and ~390 μm on day 5. Notably, cross-sectional analysis revealed a distinct pattern of cellular alignment over the 5-day culture period, indicating a dynamic microenvironment in which cells adapt to their 3D niche without forming a necrotic core.

Cells at the top and bottom surfaces were oriented parallel to the sheet plane, while the center exhibited no clear alignment. This is the first demonstration of spontaneous orientation in a self-assembled cell sheet and is likely the result of traction force distribution and mechanical equilibrium during compaction, which also contributes to the increasing thickness of the sheets over the experimental period.[58] Such alignment may support the planar geometry of the construct, while the disordered architecture in the central region may reflect dynamic microstructural reorganization to regulate overall tissue architecture and homeostasis.[59]

Moreover, the integration of a double-layer stacked construct was assessed using H&E staining. Individual cell sheets were stacked one day after formation, and the structural integrity and thickness of the resulting construct were compared to those of a single-layer sheet on day 2. As shown in Fig. S6, the two stacked sheets were fully integrated, with no visible separation or distinguishable boundary between the layers in the histological images. This observation highlights the inherent adhesive capacity of self-assembled cell sheets, which form interlayer connections through both cell–cell and cell–ECM interactions. Quantitative analysis revealed that the thickness of the double-layer construct reached approximately 182.55 ± 18.20% of that of a single-layer sheet. This result aligns with the previously observed reduction in contraction of multilayered constructs compared to single-layer sheets, potentially due to additional interfacial adhesions that mitigate contraction forces.

Collagen deposition

To assess functional activity within the self-assembled sheets, Picrosirius Red (PSR) staining was performed to evaluate collagen production after 1, 3, and 5 days of culture. Results showed a progressive increase in collagen content, occupying ~10% of the cross-sectional area on day 1, ~40% on day 3, and ~60% by day 5 (Fig. 5E). This confirms that fibroblasts within the sheets are functionally active, producing ECM components critical for tissue maturation.[59]

Compared to conventional methods that require extended 2D culture prior to sheet delamination,[1,60] our self-assembly approach enables accelerated ECM production. For instance, in a previous study, rat dermal fibroblasts required a full week on temperature-responsive culture surfaces to achieve ~32–35% collagen content before sheet detachment at 20 °C.[61] Our constructs reached similar levels within 3 days, demonstrating the efficiency and physiological relevance of the 3D self-assembled format.

Collectively, these findings validate the capability of our technique to produce structurally organized, mechanically robust, and functionally active 3D cellular constructs. The observed cytoskeletal organization, cell alignment, and enhanced ECM expression support the underlying principle that promoting cell–cell adhesion on non-adherent substrates facilitates the formation of planar, tissue-like sheets.

Assessment of cellular behaviors in cell sheet constructs

To evaluate the functional state of cells within self-assembled 3D constructs, we assessed mitochondrial metabolic activity, and total protein production in single-layer, double-layer, and triple-layer cell sheets. Results were compared to conventional 2D monolayer cultures to assess how 3D structural organization affects core cellular behaviors.

Mitochondrial metabolic activity

The mitochondrial metabolic activity of NIH/3T3 cells was analyzed using the AlamarBlue assay at various time points post-sheet formation. Single-layer cell sheets (1.5×10^6 cells per well) were compared to 2D monolayers seeded with the same cell number in standard tissue culture plates. Metabolic activity was assessed at 5 hours (early stage), day 1, and day 2 after seeding. Cells cultured in 2D exhibited consistent mitochondrial activity across all time points. In contrast, single-layer 3D cell sheets showed a significant reduction in metabolic activity, 31.75 ± 5.00% lower than 2D controls at 5 hours, and 71.81 ± 2.56% lower after one day (Fig. 6A). This disparity can be due to the structural and microenvironmental differences between the two formats. In 2D, cells spread on a rigid substrate and remain in direct contact with oxygen and nutrients, supporting high mitochondrial output. Conversely, in 3D cell sheets, cells form dense, layered structures with limited access to nutrients and oxygen, leading to lower mitochondrial activity.[62]

This early-phase suppression of mitochondrial activity likely reflects a transient, adaptive response rather than cellular dysfunction. During the initial stages of self-assembly, cells appear to redirect energy utilization away from proliferation and toward processes such as extracellular matrix production, cytoskeletal remodeling, and the stabilization of cell–cell junctions.[63] This metabolic

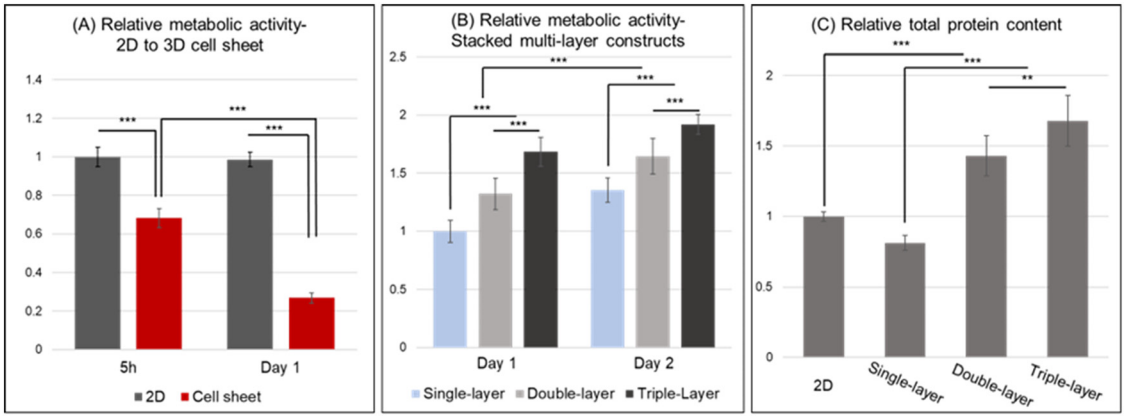

Fig. 6 Functional and molecular assessments of NIH/3T3 cell sheets. (A) Mitochondrial metabolic activity assessed shows ~30% and ~70% reduction in single-layer cell sheets at 5 h and 1 day, respectively, compared to conventional 2D culture. (B) Mitochondrial metabolic activity of single-, double-, and triple-layer constructs evaluated on days 1 and 2, normalized to single-layer values on day 1. The metabolic activity of stacked constructs is higher than single-layer, though not proportional to the number of layers—potentially due to diffusion limitations. All the groups exhibit increased activity with culture time. (C) Total protein content on day 1 reveals ~20% reduction in single-layer sheets compared to 2D controls, while stacking enhances protein content significantly. (**, ***: $p < 0.01$ and 0.001, respectively).

downregulation often reflects a quiescent-like state, where mitochondrial activity is temporarily reduced while biosynthetic and structural processes continue.[64] A reduction in mitochondrial activity does not imply a global decline in metabolism. Cells may shift to anaerobic pathways, particularly under the low-oxygen conditions common in dense 3D tissue-like constructs, to meet the biosynthetic demands of early tissue assembly.[64] Furthermore, increased tissue thickness can create diffusion gradients for oxygen, nutrients, and even metabolic dyes like AlamarBlue, potentially leading to an underestimation of mitochondrial activity, especially in inner layers.[65]

To further investigate how increasing the thickness of constructs influences mitochondrial metabolism, double-layer and triple-layer cell sheet constructs were fabricated by stacking individual NIH/3T3 cell sheets 5 hours after their initial formation. These stacked constructs, along with the single-layer cell sheet, were then incubated at 37 °C with 5% CO_2, and their mitochondrial metabolic activities were assessed on day 1 and day 2. On day 1, the double-layer constructs showed a 32.29 ± 13.48% increase in mitochondrial metabolic activity compared to single-layer sheets, while triple-layer constructs exhibited a 68.51 ± 12.44% increase (Fig. 6B). By day 2, this activity continued to rise, with double-layer constructs reaching 64.40 ± 15.34% and triple-layer constructs reaching 91.89 ± 8.55% higher metabolic activity relative to single-layer sheets at day 1. Notably, the single-layer sheets also demonstrated a 35.59 ± 10.67% increase in metabolic activity from day 1 to day 2.

While stacking multiple cell sheets to form thicker constructs leads to an increase in mitochondrial metabolic activity compared to single-layer sheets, due to the higher number of cells, this increase is not proportional to the number of stacked layers. This can be explained by the limited penetration of nutrients and oxygen through the depth of the thicker constructs, which may reduce mitochondrial metabolic activity in the early stages post-stacking.[64] However, as the culture period extends, all constructs, including single layers, undergo a time-dependent mitochondrial metabolic recovery, likely reflecting adaptation and maturation of the 3D microenvironment. As discussed earlier, initial mitochondrial suppression in 3D cell sheets is associated with cellular restructuring, hypoxia, and a temporary shift to glycolytic metabolism during early self-assembly.[64] By day 2, the observed increase in activity indicates that cells are regaining mitochondrial function as cell–cell and ECM interactions stabilize, oxygen and nutrient diffusion improves, and oxidative phosphorylation resumes.[64,66] In stacked constructs, enhanced interlayer communication and mechanical cues likely promote metabolic activation *via* ECM remodeling and mitochondrial biogenesis.[66] However, care must be taken not to exceed structural thickness limits, as excessive layering may impair diffusion and lead to central hypoxia or necrosis, as seen in other thick 3D tissues.[67]

Total protein content

To assess overall biosynthetic activity, the total protein content of single-, double-, and triple-layer cell sheets was measured and compared to 2D monolayer controls on day 1 (Fig. 6C), using PierceTM BCA Protein Assay kit. The single-layer sheet produced 81.00 ± 5.19% of the total protein content of the 2D monolayer, while double- and triple-layer constructs showed increased protein levels, reaching 142.98 ± 14.09% and 167.74 ± 18.02%, respectively. When normalized to the single-layer sheet, the total protein content values of double-layer and triple-layer constructs correspond to ~180% and ~215% of its protein content, respectively. This indicates that the double-layer construct produced slightly less than double, and the triple-layer slightly more than double, the protein amount of a single layer.

As previously mentioned, the metabolic activity of cells in 3D cell sheets decreased by about 70% relative to 2D cultures on day one. This suggests that cells within 3D sheets may enter a quiescent state, which is typically associated with reduced metabolic activity and protein synthesis.[64] It is also known that mitochondrial function regulates dynamic protein synthesis; therefore, lower mitochondrial activity in 3D cell sheet compared to 2D culture, could directly contribute to reduced biosynthetic output.[68] However, it is notable that despite the substantial reduction in mitochondrial activity, the decrease in total protein content is relatively modest. This indicates that fibroblasts in the 3D cell sheet format remain functionally active, particularly in producing their own ECM niche as the primary synthesizers of extracellular matrix components.[56] The relatively high protein production, despite lower mitochondrial metabolism, may also be attributed to the 3D culture environment. In contrast to 2D culture, where rigid substrate attachment limits spatial ECM deposition, 3D cell sheet culture permits ECM secretion in all directions, contributing to increased total protein levels.[30]

Therefore, the suitability of the 3D microenvironment may support elevated biosynthetic activity in cell sheets, even under reduced mitochondrial function.

While thicker double- and triple-layer constructs exhibited approximately 1.8- and 2.15-fold higher protein content compared to single-layer cell sheets, the increase in protein content was not proportional to the number of stacked layers. These findings align with previous observations of reduced mitochondrial activity in the early stages of 3D culture in stacked constructs compared to single-layer sheets. As previously noted, there is a direct correlation between mitochondrial activity and biosynthesis.[68] As the construct thickens with additional stacked layers, diffusion limitations to the inner regions of the tissue-like constructs can promote hypoxia and induce cellular quiescence in the deeper layers,[64] which could affect protein synthesis and reduce the total protein output of multilayer constructs at early time points (Fig. 6C).

However, our mitochondrial activity assay showed significant metabolic recovery by day 2 (Fig. 6B). Therefore, it is reasonable to expect that extended culture periods can support continued protein synthesis, allowing double- and triple-layer constructs to eventually approach or surpass the two- or threefold protein output expected based on cell number. The progressive increase in collagen deposition in single-layer cell sheets over a 5-day culture period (Fig. 5E) further supports this notion. These findings highlight the importance of culture duration and nutrient accessibility in engineering thick, high density, and functional 3D tissue constructs using cell sheets, and underscore the potential benefit of incorporating perfusion systems or vascular-like networks. Such strategies could facilitate oxygen and nutrient transport to the deeper regions of thicker constructs, promoting cellular metabolism and biosynthesis in inner layers, while reducing the risk of necrotic core formation and prolonged hypoxia.[41]

In vivo demonstration of UC-MSC sheet integration in wound

To assess the grafting potential of the self-assembled UC-MSC cell sheet, we conducted an *in vivo* demonstration using a full-thickness thermal burn wound model in a pig. The primary objective of this pilot demonstration was to examine whether the cell sheets could integrate into the wound bed without causing adverse reactions, serving as a foundational step for future investigations into therapeutic effects on wound healing and skin regeneration.

In vitro validation and *in vivo* transplantation of UC-MSC cell sheet

In this study, UC-MSCs were selected due to their known regenerative potential in wound healing, low immunogenicity, and favorable effects on re-epithelialization and neovascularization.[32]

Prior to grafting, the viability of UC-MSC sheets were assessed *in vitro*. A total of 1.5×10^6 UC-MSCs were seeded into 1 cm diameter PDMS molds and incubated at 37 °C and 5% CO_2.

Live/dead staining was performed at 5 hours and 24 hours post-seeding to confirm cell viability. Fluorescence imaging demonstrated that the majority of cells remained viable, suggesting that the self-assembly process does not negatively impact UC-MSC survival in the sheet format (Fig. S8). Then, a larger UC-MSC sheet was fabricated using 30×10^6 cells seeded into a 5 cm diameter PDMS mold. After 5 hours of incubation, a planar, patch-like structure with approximately 2.5 cm diameter formed, which was rinsed three times with Ringer's buffer to remove residual culture medium prior grafting. Next, it was transplanted onto a 5×5 cm^2 full-thickness thermal wound using flat-end spatula to partially cover the wound. No fixation (*e.g.*, sutures or staples) was required, as the sheet adhered immediately to the wound bed upon transplantation (Fig. 7). The wound site was subsequently covered with a sterile dressing throughout the observation period, wound assessments were conducted on both UC-MSC cell sheet treated wound and burn alone control sample two to three times weekly during the first three weeks, then weekly. In this preliminary demonstration of UC-MSC sheet grafting, no signs of inflammation, infection, or rejection were observed. On the first dressing change, granulation tissue formation was already visible, suggesting preliminary integration of sheet into the wound bed. Inflammation and rejection were assessed clinically, based on redness, swelling, excessive exudate, or pus formation, all of which were absent throughout the 40-day observation period (Fig. 7). However, further studies with larger samples size require to confirm these preliminary outcomes.

Preliminary histological assessment

Histological analysis was conducted on tissue biopsies collected from the center of the wounds on day 40. Samples were stained using standard hematoxylin and eosin (H&E) (Fig. 7). In the UC-MSC cell sheet-grafted wound, we observed homogeneous epidermal regeneration, including the

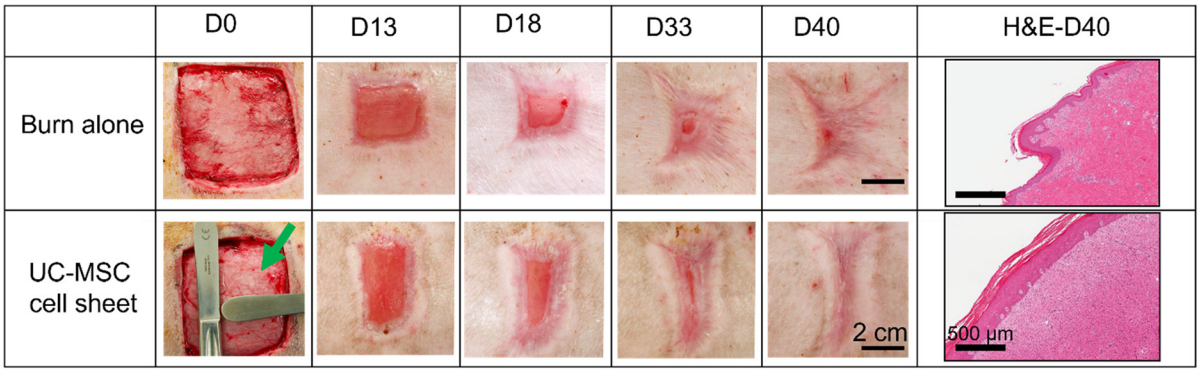

Fig. 7 Gross macroscopic images of wounds during the healing process. Photographs captured at each dressing change were used to monitor wound size and epithelialization. The grafted area of the UC-MSC cell sheet is marked by a green arrow. Scale bar: 2 cm (gross images), and 500 μm (H&E).

presence of rete ridges, and stratified epidermis composed of multiple layers of keratinocytes and a nuclei-depleted stratum corneum, features consistent with epidermal maturation. While, evidences are promising, reproducibility and repeatability of these results need to be further studied.

UC-MSCs represent a promising approach for skin regeneration, offering advantages such as low immunogenicity, enhanced ECM production, and secretion of cytokines.[32] Delivering these cells in a sheet format preserves cell–cell junctions and the native architecture of the culture, creating a biomimetic microenvironment that differs substantially from traditional scaffold-based approaches. Cell sheets maintain a planar, cohesive structure that can promote enhanced intercellular communication and cell–matrix interactions.

Furthermore, our findings from NIH/3T3 fibroblast sheets, along with prior reports,[24] suggest that the cell sheet configuration support ECM accumulation and organization. Whether UC-MSC sheets exhibit similar behaviour remains an important area for further investigation, particularly in characterizing their ECM composition and its role in wound healing. Overall, our preliminary *in vivo* results suggest that UC-MSC sheets are easy to handle, and capable of integrating into thermally injured skin. Follow-up studies with larger cohorts, and detailed microscopic and molecular analyses will be essential to fully assess the therapeutic potential and mechanisms underlying UC-MSC sheet-mediated wound repair.

Conclusions

In this study, we developed a novel and scaffold-free biofabrication technique to create planar cell sheet constructs by leveraging the natural tendency of adherent cells to form cell–cell adhesions in the absence of substrate anchorage. Cell sheet formation in this system relies on two key factors: the use of pristine, non-cell-adhesive PDMS molds with low surface energy, which inhibit cell-substrate attachment, and the application of a critical cell seeding density that ensures sufficient cell–cell contact for sheet formation rather than sparse aggregation. Upregulation of E-cadherin expression in 3D cell sheets, compared to conventional 2D cultures, supports the central role of cell–cell adhesion in driving self-assembly in this system.

Our technique allows the rapid (4–6 hours) and reproducible formation of large-area cell sheets (ranging from approximately 0.5 cm to 5 cm in diameter) in a variety of shapes and sizes using molds of different geometries. Although the contraction behavior in relation to mold size warrants further investigation, the scalability and adaptability of this platform were clearly demonstrated. Furthermore, we showed that for the fabrication of thicker and more complex tissue-like constructs, individual sheets can be layered, assembled into larger and more complicated macrostructures, or patterned to enable co-culture with multiple cell types such as HUVECs for the development of pre-vascularized cell sheets.

Extensive *in vitro* assays confirmed that the biofabrication process preserves cellular viability, supports ECM production, and maintains functionality, as evidenced by metabolic activity. A wide range of cell types including NIH/3T3, 3T3-L1, C2C12, BeWo, Saos-2, HSKMCs, BD-MSCs, UC-MSCs, NF, and Opo-Moo-M17 successfully formed robust sheets, demonstrating the versatility of the technique across diverse tissue models. Moreover, preliminary *in vivo* demonstration using UC-MSC sheet in a burn wound model showed encouraging signs of cell sheet integration to the wound bed. To fully evaluate efficacy, larger preclinical studies are essential. Future refinements, such as stacking sheets to increase thickness and incorporating removable, bioinert carriers to improve handling and graft protection, represent important steps toward clinical translation.

Altogether, the approach described here offers a rapid, cost-effective, and user-friendly alternative to existing cell sheet biofabrication methods. By removing the need for surface treatments, enzymatic detachment, or specialized equipment, it provides a versatile platform with strong potential for applications in tissue engineering, regenerative medicine, *in vitro* modeling, drug screening, and cultivated meat production.

Author contributions

Maedeh Khodamoradi: conceptualization, data curation, formal analysis, investigation, methodology, project administration, validation, visualization, writing – original draft. Seyedaydin Jalali: formal analysis, methodology, visualization, writing – review and editing. Maria Fernanda Hutter: data curation, formal analysis, investigation, writing – original draft. Yufei (Andy) Chen: formal analysis. Faraz Chogan: visualization. Alisa Douglas: investigation. Graham Rix: investigation. Bhavishya Challagundla: investigation. Margarita Elloso: formal analysis, writing – original draft. Marc G. Jeschke: supervision, validation, writing – review and editing. Ponnambalam R. Selvaganapathy: conceptualization, funding acquisition, supervision, validation, writing – review and editing.

Conflicts of interest

There are no conflicts to declare.

Data availability

Data related to the manuscript has been provided both in the manuscript and the supplementary information (SI) section. Supplementary information is available. See DOI: https://doi.org/10.1039/d5lc00678c.

Acknowledgements

Some of the *in vitro* assessments were performed at the Biointerfaces Institute (BI) at McMaster University. High resolution confocal micrographs were taken at the Center of Advanced Light Microscopy (CALM) at McMaster University. C2C12 and BeWo cells that were used in this study were kindly provided by Dr. Sandeep Raha Department of Pediatrics, McMaster University. BD-MSCs, UC-MSCs, and NF cells were also kindly provided by Dr. Marc G. Jeschke Professor, Surgery, Faculty of Health Sciences, McMaster University. Dr. Selvaganapathy acknowledges support from the Joseph and Amy Chair in Bioinnovation.

Notes and references

1 A. De Pieri, Y. Rochev and D. I. Zeugolis, *npj Regener. Med.*, 2021, **6**(1), DOI: 10.1038/s41536-021-00133-3.
2 M. Salvadori, N. Cesari, A. Murgia, P. Puccini, B. Riccardi and M. Dominici, *Mol. Ther.–Methods Clin. Dev.*, 2019, **14**, 1–15.
3 J. A. Burdick, R. L. Mauck and S. Gerecht, *Cell Stem Cell*, 2016, **18**, 13–15.
4 Y. Li, M. Zhou, W. Zheng, J. Yang and N. Jiang, *Regener. Biomater.*, 2023, **10**, DOI: 10.1093/rb/rbac091.
5 S. You, Y. Xiang, H. H. Hwang, D. B. Berry, W. Kiratitanaporn, J. Guan, E. Yao, M. Tang, Z. Zhong, X. Ma, D. Wangpraseurt, Y. Sun, T. Lu and S. Chen, *Sci. Adv.*, 2023, **9**(8), DOI: 10.1126/sciadv.ade7923.
6 J. D. Enderle and J. D. Bronzino, *Introduction to biomedical engineering*, Academic Press, 2012.
7 K. A. Athanasiou, R. Eswaramoorthy, P. Hadidi and J. C. Hu, *Annu. Rev. Biomed. Eng.*, 2013, **15**, DOI: 10.1146/annurev-bioeng-071812-152423.
8 E. Fennema, N. Rivron, J. Rouwkema, C. van Blitterswijk and J. de Boer, *Trends Biotechnol.*, 2013, **31**, 108–115.
9 D. Fayol, G. Frasca, C. Le Visage, F. Gazeau, N. Luciani and C. Wilhelm, *Adv. Mater.*, 2013, **25**, 2611–2616.
10 K. Matsuura, R. Utoh, K. Nagase and T. Okano, *J. Controlled Release*, 2014, **190**, 228–239.
11 H. Byun, Y. Bin Lee, E. M. Kim and H. Shin, *Biofabrication*, 2019, **11**, 035025.
12 N. Di Caprio and J. A. Burdick, *Acta Biomater.*, 2023, **165**, 4–18.
13 A. M. Bratt-Leal, K. L. Kepple, R. L. Carpenedo, M. T. Cooke and T. C. McDevitt, *Integr. Biol.*, 2011, **3**, 1224–1232.
14 A. Shahin-Shamsabadi and P. R. Selvaganapathy, *ACS Biomater. Sci. Eng.*, 2020, **6**, 5346–5356.
15 J. P. Frampton, B. M. Leung, E. L. Bingham, S. C. Lesher-Perez, J. D. Wang, H. T. Sarhan, M. E. H. El-Sayed, S. E. Feinberg and S. Takayama, *Adv. Funct. Mater.*, 2015, **25**, 1694–1699.
16 M. Kondo, S. Kameishi, K. Kim, N. F. Metzler, T. G. Maak, D. T. Hutchinson, A. A. Wang, M. Maehara, M. Sato, D. W. Grainger and T. Okano, *npj Regener. Med.*, 2021, **6**, 1–11.
17 N. Asakawa, T. Shimizu, Y. Tsuda, S. Sekiya, T. Sasagawa, M. Yamato, F. Fukai and T. Okano, *Biomaterials*, 2010, **31**, 3903–3909.
18 H. Lee, J. H. Lee, S. Hong, J. H. Sunwoo, H. T. Kim, E. Kim, J. Y. Kim, C. Hwang and H. Tchah, *J. Tissue Eng. Regener. Med.*, 2021, **15**, 139–149.
19 M. N. Ahmed, D. Shi, M. T. Dailey, K. Rothermund, M. D. Drewry, T. C. Calabrese, X. T. Cui and F. N. Syed-Picard, *Tissue Eng., Part A*, 2021, **27**, 1128–1139.
20 H. Thorp, K. Kim, S. Bou-Ghannam, M. Kondo, T. Maak, D. W. Grainger and T. Okano, *Regener. Ther.*, 2021, **18**, 487–496.
21 J. M. Unagolla and A. C. Jayasuriya, *Appl. Mater. Today*, 2020, **18**, 100479.
22 A. M. de Leeuw, R. Graf, P. J. Lim, J. Zhang, G. N. Schädli, S. Peterhans, M. Rohrbach, C. Giunta, M. Rüger, M. Rubert and R. Müller, *Front. Bioeng. Biotechnol.*, 2024, **12**, 1310289.
23 G. N. Schädli, J. R. Vetsch, R. P. Baumann, A. M. de Leeuw, E. Wehrle, M. Rubert and R. Müller, *Commun. Biol.*, 2021, **4**(1), 110.
24 P. Thummarati, W. Laiwattanapaisal, R. Nitta, M. Fukuda, A. Hassametto and M. Kino-oka, *Bioengineering*, 2023, **10**, 211.
25 M. S. Singh, S. S. Park, T. A. Albini, M. V. Canto-Soler, H. Klassen, R. E. MacLaren, M. Takahashi, A. Nagiel, S. D. Schwartz and K. Bharti, *Prog. Retin. Eye Res.*, 2020, **75**(3), DOI: 10.1016/J.PRETEYERES.2019.100779.
26 Z. Tang, Y. Akiyama and T. Okano, *Polymers*, 2012, **4**, 1478–1498.
27 O. Guillaume-Gentil, O. V. Semenov, A. H. Zisch, R. Zimmermann, J. Vörös and M. Ehrbar, *Biomaterials*, 2011, **32**, 4376–4384.

28 Y. Kobayashi, C. E. J. Cordonier, Y. Noda, F. Nagase, J. Enomoto, T. Kageyama, H. Honma, S. Maruo and J. Fukuda, *Sci. Rep.*, 2019, **9**, 10415.
29 Y. Hong, M. Yu, W. Weng, K. Cheng, H. Wang and J. Lin, *Biomaterials*, 2013, **34**, 11–18.
30 K. Duval, H. Grover, L.-H. Han, Y. Mou, A. F. Pegoraro, J. Fredberg and Z. Chen, *Physiology*, 2017, **32**, 266–277.
31 S. Jalali and P. R. Selvaganapathy, *Lab Chip*, 2024, **24**, 2468–2484.
32 G. Eylert, R. Dolp, A. Parousis, R. Cheng, C. Auger, M. Holter, I. Lang-Olip, V. Reiner, L. P. Kamolz and M. G. Jeschke, *Stem Cell Res. Ther.*, 2021, **12**(1), DOI: 10.1186/s13287-020-02131-6.
33 Y. Shang, H. Guan and F. Zhou, *Front. Cell Dev. Biol.*, 2021, **9**(5), DOI: 10.3389/fcell.2021.570179.
34 B. M. Baker and C. S. Chen, *J. Cell Sci.*, 2012, **13**(7), DOI: 10.1242/jcs.079509.
35 S. Kim, E. M. Kim, M. Yamamoto, H. Park and H. Shin, *Adv. Healthcare Mater.*, 2020, **9**(23), DOI: 10.1002/adhm.202000608.
36 D. H. Yang, S. Jung, J. Y. Kim and N. Y. Lee, *Micromachines*, 2022, **13**, 1122.
37 S. Vudayagiri, M. D. Junker and A. L. Skov, *Polym. J.*, 2013, **45**, 871–878.
38 S. Kim, H. Choi, S. Jin, S. Son, Y. Lee, K. Kim and J.-H. Ryu, *Giant*, 2023, **16**, 100189.
39 L. S. Price, A. Hajdo-Milasinovic, J. Zhao, F. J. T. Zwartkruis, J. G. Collard and J. L. Bos, *J. Biol. Chem.*, 2004, **279**, 35127–35132.
40 S. L. Dalton, E. Scharf, R. Briesewitz, E. E. Marcantonio and R. K. Assoian, *Cell Adhesion to Extracellular Matrix Regulates the Life Cycle of Integrins*, 1995, vol. 6.
41 K. Moschouris, N. Firoozi and Y. Kang, *Regener. Med.*, 2016, DOI: 10.2217/rme-2016-0059.
42 A. De Pieri, Y. Rochev and D. I. Zeugolis, *NPJ Regen Med.*, 2021, **6**, 18.
43 Y. M. Efremov, I. M. Zurina, V. S. Presniakova, N. V. Kosheleva, D. V. Butnaru, A. A. Svistunov, Y. A. Rochev and P. S. Timashev, *Biophys. Rev.*, 2021, **13**, 541–561.
44 T. Takezawa, Y. Mori and K. Yoshizato, *Nat. Biotechnol.*, 1990, **8**, 854–856.
45 T. Xie, S. R. St Pierre, N. Olaranont, L. E. Brown, M. Wu and Y. Sun, *Elife*, 2021, **10**(9), DOI: 10.7554/eLife.60381.
46 R. Costa-Almeida, M. Gomez-Lazaro, C. Ramalho, P. L. Granja, R. Soares and S. G. Guerreiro, *Tissue Eng. Part A*, 2015, **21**, 1055–1065.
47 L. T. Hung, S. H. L. Poon, W. H. Yan, R. Lace, L. Zhou, J. K. W. Wong, R. L. Williams, K. C. Shih, H. C. Shum and Y. K. Chan, *ACS Biomater. Sci. Eng.*, 2022, **8**, 1987–1999.
48 D. Larouche, L. Cantin-Warren, M. Desgagné, R. Guignard, I. Martel, A. Ayoub, A. Lavoie, R. Gauvin, F. A. Auger, V. J. Moulin and L. Germain, *BioRes Open Access*, 2016, **5**, 320–329.
49 I. E. Hannachi, M. Yamato and T. Okano, *Biofabrication*, 2009, **1**, 022002.
50 S. Kusuma, S. Zhao and S. Gerecht, *FASEB J.*, 2012, **26**, 4925–4936.
51 R. Attalla, E. Puersten, N. Jain and P. R. Selvaganapathy, *Biofabrication*, 2018, **11**, 015012.
52 W. Ramadhan, G. Kagawa, K. Moriyama, R. Wakabayashi, K. Minamihata, M. Goto and N. Kamiya, *Sci. Rep.*, 2020, **10**, 6710.
53 H. Sekine, T. Shimizu, K. Sakaguchi, I. Dobashi, M. Wada, M. Yamato, E. Kobayashi, M. Umezu and T. Okano, *Nat. Commun.*, 2013, **4**(1), DOI: 10.1038/ncomms2406.
54 T. Sasagawa, T. Shimizu, S. Sekiya, Y. Haraguchi, M. Yamato, Y. Sawa and T. Okano, *Biomaterials*, 2010, **31**, 1646–1654.
55 M. S. Kim, B. Lee, H. N. Kim, S. Bang, H. S. Yang, S. M. Kang, K.-Y. Suh, S.-H. Park and N. L. Jeon, *Biofabrication*, 2017, **9**, 015029.
56 M. V. Plikus, X. Wang, S. Sinha, E. Forte, S. M. Thompson, E. L. Herzog, R. R. Driskell, N. Rosenthal, J. Biernaskie and V. Horsley, *Cell*, 2021, **184**, 3852–3872.
57 S. Bou-Ghannam, K. Kim, D. W. Grainger and T. Okano, *Sci. Rep.*, 2021, **11**, 8170.
58 M. Lekka, K. Gnanachandran, A. Kubiak, T. Zieliński and J. Zemła, *Micron*, 2021, **150**, 103138.
59 L. A. Murray, D. A. Knight and G. J. Laurent, in *Asthma and COPD*, Elsevier, 2009, pp. 193–200.
60 Z. Qian, D. Ross, W. Jia, Q. Xing and F. Zhao, *Bioact. Mater.*, 2018, **3**, 167–173.
61 T. Nozaki, M. Yamato, T. Inuma, K. Nishida and T. Okano, *J. Tissue Eng. Regen. Med.*, 2008, **2**, 190–195.
62 T. Takezawa, Y. Mori, T. Yonaha and K. Yoshizato, *Exp. Cell Res.*, 1993, **208**, 430–441.
63 Y. Bin Lee, E. M. Kim, H. Byun, H. Chang, K. Jeong, Z. M. Aman, Y. S. Choi, J. Park and H. Shin, *Biomaterials*, 2018, **165**, 105–120.
64 O. Marescal and I. M. Cheeseman, *Dev. Cell.*, 2020, DOI: 10.1016/j.devcel.2020.09.029.
65 O. Urzì, R. Gasparro, E. Costanzo, A. De Luca, G. Giavaresi, S. Fontana and R. Alessandro, *Int. J. Mol. Sci.*, 2023, **24**, 12046.
66 M. Ouyang, Y. Hu, W. Chen, H. Li, Y. Ji, L. Qiu, L. Zhu, B. Ji, B. Bu and L. Deng, *Research*, 2023, **6**(1), DOI: 10.34133/research.0270.
67 L. G. Griffith and M. A. Swartz, *Nat. Rev. Mol. Cell Biol.*, 2006, **7**, 211–224.
68 Y. Zong, H. Li, P. Liao, L. Chen, Y. Pan, Y. Zheng, C. Zhang, D. Liu, M. Zheng and J. Gao, *Signal Transduction Targeted Ther.*, 2024, **9**, 124.